J. Fluid Mech. (1982), *vol.* 118, *pp.* 471–505
Printed in Great Britain

Measurement of fluid turbulence based on pulsed ultrasound techniques. Part 2. Experimental investigation

By JOSEPH L. GARBINI, FRED K. FORSTER† AND JENS E. JORGENSEN

Department of Mechanical Engineering,
University of Washington, Seattle, U.S.A.

(Received 27 February 1981 and in revised form 30 September 1981)

An extensive experimental programme in both laminar and turbulent flow was undertaken to examine the validity of all of the major implications of the model of the pulsed ultrasonic Doppler velocimeter for turbulent flow developed in part 1 of this investigation. The turbulence measurements were made in fully developed flow at the centre of a 6·28 cm diameter pipe. The Reynolds number of the flow ranged from 6000 to 40000. The carrier frequency of the ultrasonic velocimeter was 4·7 MHz.

Measurements of the turbulence intensity and of the one-dimensional velocity spectra made with the ultrasonic velocimeter are compared with the analysis and with the actual quantities as measured by a hot-film anemometer. The experimental results are in agreement with theoretical predictions.

Measurements of one-dimensional turbulence spectra with reduced ambiguity spectra made by the two sample volume methods described in part 1 are presented. The results verify the analysis and indicate that an improvement in the useful dynamic range of the velocity power spectrum of nearly three orders of magnitude can realistically be achieved.

1. Introduction

Establishment of the pulsed ultrasonic Doppler velocimeter as a reliable tool for the evaluation of turbulence requires that a reasonable level of confidence be gained in the description of its characteristics and limitations in well-defined situations. The experimental programme that has been carried out and is described in the following sections was aimed both at verification of the theoretical results of the study (Garbini, Forster & Jorgensen 1982, hereinafter referred to as part 1) and at revealing any inadequacies in that analysis.

The laboratory investigation may be broadly divided into four parts. In the first portion, model parameters, principally the sample-volume dimensions, and the spectrum of the Doppler-ambiguity process were determined. Of the two causes of ambiguity discussed in § 2.3 of part 1 it will be seen that the transit-time effect, which is associated with the mean velocity rather than the velocity fluctuations, is usually dominant. Therefore this effect was isolated by measuring the detected velocity signal spectrum in steady, uniform, laminar flow. For an ideal velocity-measuring

† Also at Center for Bioengineering, University of Washington, Seattle.

device the spectrum should be zero at all frequencies greater than zero. For the ultrasonic Doppler velocimeter this result corresponds to the velocity-ambiguity process. These spectral measurements were compared with the theoretical predictions of the ambiguity spectrum based on the Gaussian-shaped sample-volume model.

In the second part, one-dimensional energy spectra for turbulent flow were measured. The test situation selected for this evaluation was that of fully developed turbulent flow at the centre of a pipe. These measurements were made over a wide range of Reynolds numbers. All major implications of the model were investigated experimentally. The results demonstrate clearly the limitations of the ultrasonic velocimeter in turbulent flow. The ultrasonic measurements were compared directly with those obtained using a hot-film anemometer and with theoretical predictions of the Doppler velocimeter output based upon the model. The turbulence intensities were also evaluated from the width of the Doppler spectrum and compared with hot-film measurements.

The third and fourth parts of the experimental programme dealt with the reduction of the velocity-ambiguity process by means of the dual-sample-volume cross-spectra technique. For the preliminary measurements, flat-profile laminar flow was again used to isolate the Doppler-ambiguity phenomenon. Measurements were made of cross-spectra of the detected velocity signals from two sample volumes in laminar flow for selected spacings and Doppler angles. In this way the effects of overlap and shadowing, as described in § 3, were examined empirically. These results were compared with theoretical predictions based on the Gaussian-shaped sample-volume approximation.

In the final experiments, the dual-sample-volume cross-spectrum method was evaluated in turbulent flow. The results of the laminar-flow experiments were used to arrange the sample volumes in near-optimal configurations with respect to the effects of sample-volume overlap and shadowing. The resulting one-dimensional velocity spectrum estimates were compared with the hot-film measurements for overall accuracy. The total reduction in the ambiguity process was evaluated by comparison of these results with those of the single-sample-volume measurements.

2. Data-reduction techniques

2.1. *Demodulation of the Doppler signal*

In § 2.3 of part 1 it was shown that an estimate of the one-dimensional turbulence spectrum may be obtained from properly scaled computation of the power spectrum of the instantaneous rate of change of phase of the Doppler signal. This detected velocity signal is of the form:

$$\omega_{\mathrm{d}} = \mathbf{k} \,.\, \langle \mathbf{u} \rangle + \dot{\Phi}, \tag{2.1}$$

where $\mathbf{k}$ is the Doppler wave vector, $\langle \mathbf{u} \rangle$ is the spatial average velocity and $\dot{\Phi}$ is the ambiguity process. The problem of obtaining this signal from the Doppler signal is analogous to that of FM detection. In practice, a phase-locked loop demodulator or a zero-crossing detector is usually used to determine the detected velocity signal. Quite often these devices suffer from bias errors inherent in the technique, or from limitations in frequency response for wide-band signals (Angelsen & Kristoffersen 1979). Since the turbulent fluctuations in velocity are small and since the bandwidth of the Doppler signal is large, such restrictions are significant.

For the purposes of this investigation it proved both convenient and accurate to

determine the detected velocity signal by computing directly the instantaneous rate of change of phase of the digitized Doppler signal. It can be shown (Garbini 1978) that the detected velocity signal can be expressed as

$$\mathbf{k}\,.\,\langle\mathbf{u}\rangle+\dot{\Phi}(t)=\frac{\mathscr{H}[x]\,\dot{x}-x\mathscr{H}[\dot{x}]}{x^2+\mathscr{H}[x]^2}, \tag{2.2}$$

where $\mathscr{H}(x)$ denotes the Hilbert transform of the Doppler signal $x(t)$. Specifications for optimal numerical realizations for the Hilbert and derivative transforms are well developed in the literature (Rabiner & Schafer 1974*a*, *b*, *c*; Oppenheim & Schafer 1975).

2.2. *Spectral analysis*

The results of this investigation include estimates of the power-spectral densities of the hot-film and Doppler signals. In addition, both the power and cross-spectral densities of the detected velocity signals must be computed. The two-sided spectral density of two stationary random processes $x(t)$ and $y(t)$ is defined by

$$S_{xy}(\omega)=\int_{-\infty}^{+\infty}R_{xy}(\tau)\,e^{-i\omega\tau}\,d\tau, \tag{2.3}$$

and the one-sided spectral-density function by

$$G_{xy}(\omega)=2\int_{-\infty}^{+\infty}R_{xy}(\tau)\,e^{-i\omega\tau}\,d\tau, \tag{2.4}$$

where $R_{xy}(\tau)$ is the correlation function of the two processes.

In all cases fast-Fourier-transform techniques were used to compute the spectral-density estimate from digitized records of the time series.

When $x(t)$ and $y(t)$ are the same process the digital raw autospectral estimate is

$$\tilde{G}_k=\frac{2}{N\Delta t}|X_k|^2, \tag{2.5}$$

where

$$X_k=\sum_{n=0}^{N-1}x_n\exp\left(-i\frac{2\pi kn}{N}\right)\quad(k=0,1,\ldots,N-1). \tag{2.6}$$

x_n is the digitized record of a sample function of the process $x(t)$, N is the number of points in x, and Δt is the digitization interval.

The standard deviation of the estimate is at least of order equal to the amplitude of the actual spectrum itself. More precisely,

$$\mathrm{var}\,[\tilde{G}_k]=G^2(K\Delta f)\left[1+\frac{K_4}{\sigma^4N}\right], \tag{2.7}$$

where σ^2 and K_4 are respectively the variance and fourth cumulant of the process $x(t)$. Averaging of individual spectral estimates followed by (moving-average) frequency smoothing was used to reduce the variance of the final spectral estimates (Bendat & Piersol 1971).

For a Gaussian random process K_4 is zero, and the spectral-density estimates just described are approximately chi-squared variables. The $100\,(1-\alpha)\,\%$ confidence interval is described as (Koopmans 1974)

$$\left[\frac{\nu G(k\Delta f)}{\chi^2_\nu(1-\frac{1}{2}\alpha)},\frac{\nu G(k\Delta f)}{\chi^2_\nu(\frac{1}{2}\alpha)}\right], \tag{2.8}$$

where ν is the number of degrees of freedom associated with the variance reduction technique used. When plotted on logarithmic scales the confidence limits are represented as constant length intervals around the spectral estimate.

It was established in § 2.1 of part 1 that the Doppler signal is a Gaussian random process. Therefore the preceding discussion is valid for the estimate of the spectrum of that quantity, and the confidence limits were established accordingly.

Although the turbulent-velocity fluctuations are not Gaussian, the value of the fourth cumulant for isotropic turbulence is known to be small in comparison with σ^4 (Monin & Yaglom 1975). From (2.7), for large N, the variance of the spectral estimate asymptotically approaches the value for the Gaussian case. Therefore the confidence intervals for the spectra of the hot-film anomometer measurements of the turbulence were also determined by (2.8).

The final distinct random process to be considered is the Doppler ambiguity $\dot{\Phi}$. The probability-density function of a process of this type was established by Rice (1949) to be

$$P(\dot{\Phi}) = \frac{1}{2\sigma_s(1+\dot{\Phi}^2/\sigma_s^2)^{\frac{3}{2}}}, \tag{2.9}$$

where σ_s^2, for this particular application, corresponds to the width of the Doppler spectrum. The ratio of the fourth cumulant to the square of the variance for such a function is infinite. Therefore the theoretical variance of the spectral estimate, according to (2.7), would be infinite. Of course, in any practical determination, the range of the random variable is limited to a finite region about its mean. Such a restriction forces the value of K_4/σ^4 to be finite. Therefore the confidence intervals will approach those of equation (2.8) for large N.

The cross-correlation estimates required by the dual-sample-volume ambiguity reduction technique (§ 4) were computed according to

$$\tilde{G}_{xy_k} = \frac{2}{N\Delta t}[X_k^* Y_k], \tag{2.10}$$

where X and Y are respectively the discrete fast Fourier transforms of the two random processes, and $*$ denotes the complex conjugate. The variance of such an estimate depends upon the coherency of the two processes, as well as the respective amplitudes. For approximately normal processes the relation is (Jenkins & Watts 1968)

$$\text{var}\,[\tilde{G}_{xy_k}] = \sigma_{xy}^2(1+1/k_{xy}^2), \tag{2.11}$$

where σ_{xy} is the cross-spectral amplitude $|G_{xy}(f)|$, and k_{xy}^2 is the squared coherency. Since the ambiguity-process portions of the detected velocity signal from the two sample volumes are largely uncorrelated, the coherency is low. Therefore the variance of the spectral estimates is high over portions of the frequency range. This necessitates additional use of the smoothing techniques described earlier. No attempt was made to establish precise confidence intervals for the cross-correlation estimates.

The graphs of experimentally derived power spectral estimates presented in the following sections are accompanied by the parameters describing the spectral-estimation procedure, and, where appropriate, the confidence intervals.

2.3. *Spectral moment and intensity measurement*

In § 3.3, hot-film measurements of the turbulence intensity at the centre of the pipe are compared with those made with the pulsed ultrasonic Doppler velocimeter. The intensity estimates for the hot-film anemometer may be computed from the one-dimensional energy spectrum according to

$$I = \frac{(\overline{u'^2})^{\frac{1}{2}}}{\overline{U}} = \frac{1}{\overline{U}} \int_0^{+\infty} E(k_1)\, dk_1, \tag{2.12}$$

where $E(k_1)$, in turn, is estimated from the smoothed, properly scaled, one-sided, spectral estimate of the anemometer bridge voltage. That is,

$$\hat{E}(k_1) = \frac{\overline{U}}{2\pi} \hat{G}_k. \tag{2.13}$$

The analogous computation for the ultrasonic Doppler velocimeter would involve the integral of the estimation of the spectrum of the detected velocity signal. However, in § 2.3 of part 1 it was shown that this signal contains a random ambiguity process in addition to the velocity fluctuations. The mean-square value of this spectrum is meaningless.

However, it was also shown in § 2.2 of part 1 that the intensity of the velocity fluctuations is related to the moments of the Doppler signal spectrum according to

$$I = \left[\left(\frac{\sigma_s}{\bar{f}} \right)^2 \cos^2 \theta - \alpha^2 \right]^{\frac{1}{2}}, \tag{2.14}$$

where σ_s is the variance of the Doppler signal spectrum $G(f)$, defined by

$$\sigma_s^2 = \frac{\int_0^\infty (f-\bar{f})^2 G(f)\, df}{\int_0^\infty G(f)\, df}; \tag{2.15}$$

$\bar{f}$ is the mean of the Doppler signal spectrum,

$$\bar{f} = \frac{\int_0^\infty f G(f)\, df;}{\int_0^\infty G(f)\, df}; \tag{2.16}$$

and α is a parameter descriptive of the particular ultrasonic instrument,

$$\alpha = \frac{\lambda}{4 \times 2^{\frac{1}{2}} \pi \sigma_v}, \tag{2.17}$$

where λ is the wavelength of the acoustic carrier and σ_v is the dimension of the sample volume in the direction of the mean velocity.

As a practical matter, there are several important considerations in attempting to use these relations to determine the intensity. First the $(f-\bar{f})^2$ factor in the integrand of (2.15) causes the calculation of σ_s to be very sensitive to noise components in the estimate of $G(f)$. This problem may be alleviated by limiting the interval of integration to a finite region about the spectral mean.

An important consideration in determining the intensity is the variance of the calculation itself. Equation (2.14) requires that σ_s^2/f^2 be estimated. Equations (2.15), (2.16) and simple numerical integration yield

$$(\sigma_s^2/\bar{f}^2) = \frac{(\sum_k k^2\hat{G}_k)(\sum_k \hat{G}_k)}{\sum_k k\hat{G}_k} - 1. \tag{2.18}$$

From (2.18) and (2.14) the error in the estimate of the intensity depends upon the accuracy of the spectral estimates $\hat{G}_k$, the number of points in the summation ($\frac{1}{2}N$), the parameter α associated with the instrument, and the value of the intensity. The sensitivity of the calculation to these factors can be explored by evaluating the normalized standard error, defined by

$$\epsilon = \frac{E\{(\hat{I}-I)^2\}^{\frac{1}{2}}}{I} = \frac{E\{[((\sigma_s/f)^2\cos^2\theta - \alpha^2)^{\frac{1}{2}} - I]^2\}^{\frac{1}{2}}}{I}. \tag{2.19}$$

This expression may be evaluated approximately by expanding the expectation in a Taylor series about the actual value of the intensity, and retaining only the first-order terms. Assuming that the elements of the spectral estimate of the Doppler signal are uncorrelated, the normalized standard error is

$$\frac{[E\{(\hat{I}-I)^2\}]^{\frac{1}{2}}}{I} = \frac{1}{2I^2}\left[\sum_{k=1}^{\frac{1}{2}N}\left\{\left(\sum_n^{\frac{1}{2}N} f_n G_n\right)^2\left[\sum_n^{\frac{1}{2}N} f_n^2 G_n + f_k^2\sum_n^{\frac{1}{2}N} G_n\right]\right.\right.$$
$$\left.\left. - 2f_k\left[\sum_n^{\frac{1}{2}N} f_n^2 G_n\right]\left[\sum_n^{\frac{1}{2}N} G_n\right]\left[\sum_u^{\frac{1}{2}N} f_n G_n\right]\right\}^2 \frac{\mathrm{var}\,[\hat{G}_k]}{\left(\sum_n^{\frac{1}{2}N} f_n G_n\right)^8}\right]^{\frac{1}{2}}. \tag{2.20}$$

For the discrete Fourier-transform method of spectral estimation described in § 2.2 the variance is approximately $\mathrm{var}\,[\hat{G}_k] = G(k\Delta f)^2/M$, where $2M$ is the number of degrees of freedom. Assuming that the sampling rate of the Doppler signal is four times the mean frequency, and that N is large, the summations in (2.20) may be replaced by the corresponding integral quantities. If the Doppler spectrum is described by the Gaussian shapes derived in part 1 then the normalized error for the intensity estimate is given by

$$\frac{(MN)^{\frac{1}{2}}E\{(\hat{I}-I)^2\}^{\frac{1}{2}}}{I} = \left(\frac{1}{2\pi}\right)^{\frac{1}{2}}\frac{\bar{f}\cos^2\theta}{\sigma_s I^2}\left\{\int_0^\infty\left[\bar{f}^2 - 2\bar{f}\left(\left(\frac{\sigma_s}{\bar{f}}\right)^2+1\right)\right.\right.$$
$$\left.\left. + \left(\left(\frac{\sigma_s}{\bar{f}}\right)^2+1\right)\right]^2 \exp\left(-\left[\frac{\bar{f}-1}{\sigma_s/\bar{f}}\right]^2\right) d\bar{f}\right\}^{\frac{1}{2}}. \tag{2.21}$$

This expression is plotted in figure 1 as a function of intensity, for several values of the parameter α.

There are several significant qualitative characteristics of the function. First, for any α, the expected value of the error decreases rapidly at low values of the intensity. Therefore as the intensity decreases it is necessary to increase the number of degrees of freedom in the spectral estimate or the number of points in each sampled segment. In addition, the error is reduced for large values of σ_v/λ. Therefore it is also desirable that the dimension of the sample volume in the direction of the mean flow be large compared with the carrier wavelength.

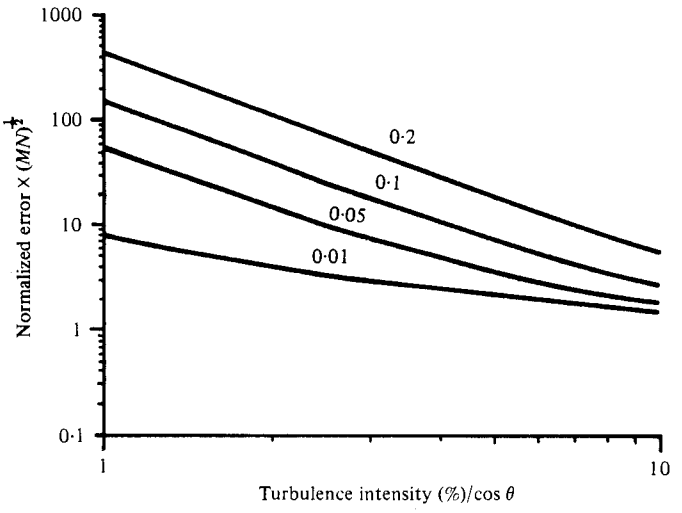

FIGURE 1. Normalized error for the calculation of the intensity as a function of the instrument and estimation parameters. N = samples/record. M = records averaged in the spectral estimate. The parameter $\alpha/\cos\theta$ = 0·01, 0·05, 0·1 and 0·2.

For the particular ultrasonic device and Doppler angle used in the intensity experiments described in the following sections, the value of the parameter was equal to 0·04, and the Doppler angle was 45°. The intensity measurements were computed from Doppler signal spectrum estimations containing 300 degrees of freedom with 1024 points per sampled segment. The smallest value of the turbulence intensity measured was approximately 3·5 %. Therefore from figure 1 the normalized standard error of these estimates was of the order of 1·0 %.

2.4. *Equipment and experimental procedure*

The laminar-flow system. The laminar and turbulent portions of the experimental procedures described in the following sections were carried out in separate flow systems. The laminar flow system was used both for the evaluation of the non-turbulent effects on the detected velocity signal spectrum and for calibration of the hot-film anemometer probe. The flow system consists of a contraction section with circular symmetry which exists into a test tank where the ultrasonic transducer or hot-film probe is located (see figure 2). The flow at the 2·54 cm throat of this contraction was laminar and was free of significant velocity gradients in the transverse direction.

Turbulent-flow system. To evaluate the accuracy of the theoretical description of the Doppler velocimeter for turbulence measurements, the test situation chosen was that of fully developed turbulent flow in a pipe. A principal advantage of this configuration is that a large body of experimental results using hot-film and laser anemometers have been reported in the literature. These data provide a convenient check on the data taken here. In addition, since the velocity profile at the centre of the pipe is nearly flat, the effects of gradients may be avoided. Finally, the turbulence in the core region is known to be approximately isotropic (Laufer 1954; Sandborn 1954).

The evaluation of the theory consists of a comparison between the Doppler velocimeter measurements and known results for the range of Reynolds numbers from 5000 to 40 000. Since the measurements of turbulence spectra, intensities and scales reported

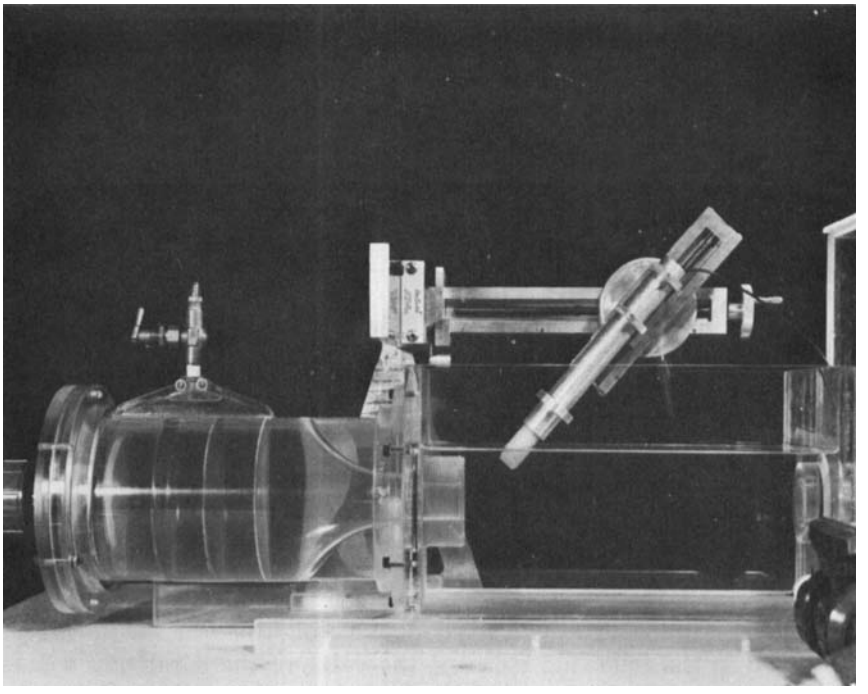

FIGURE 2. The laminar-flow facility.

in the literature are incomplete in part of this range, it was necessary to fill in this information with additional hot-film measurements.

A diagram and photographs of the flow system are shown in figures 3 and 4. The tube is aluminium, 625 cm in length, with internal diameter of to 6·18 cm. The ultrasonic and hot-film measurements were made five diameters from the end of the tube. The test section is fitted with ports that hold the ultrasonic transducer at various Doppler angles with respect to the flow.

As discussed in § 1.2 of part 1, the ultrasonic Doppler velocimeter used in these experiments incorporates a sinusoidal carrier and coherent mixing demodulation, which results in a serious range ambiguity. Normally, the acoustic beam would be reflected from the far wall of the tube, resulting in a series of sample volumes in the flow in addition to the one at the tube centre. The spacing of these sample volumes, determined by the pulse-repetition frequency f_{rp}, is $c/2f_{\mathrm{rp}}$. To eliminate these reflections the section of the pipe just upstream of the point of measurement was made of ρc-rubber. Since the characteristic acoustic impedance matches that of water, nearly all of the acoustic energy is transmitted into the rubber, where it is absorbed.

Doppler velocimeter (processor and transducers). A block diagram of the pulsed ultrasonic Doppler velocimeter used in this investigation is shown in figure 5. This instrument incorporated a single-crystal transducer, coherent-mixing demodulation and sample-and-hold gating circuits. As illustrated, the back-scattered signal is multiplied in the mixer by master oscillator signals. This provides Doppler signals for subsequent processing of the observed velocity. Two gating circuits were used to produce Doppler signals from two sample volumes that can be separated along the acoustic beam. This was accomplished by delaying the activation of one gate relative

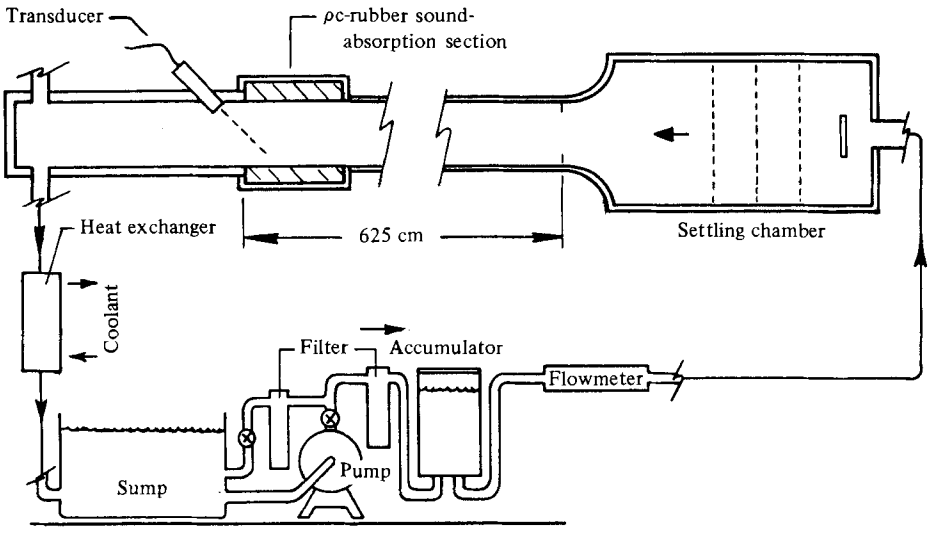

FIGURE 3. The turbulent-flow facility.

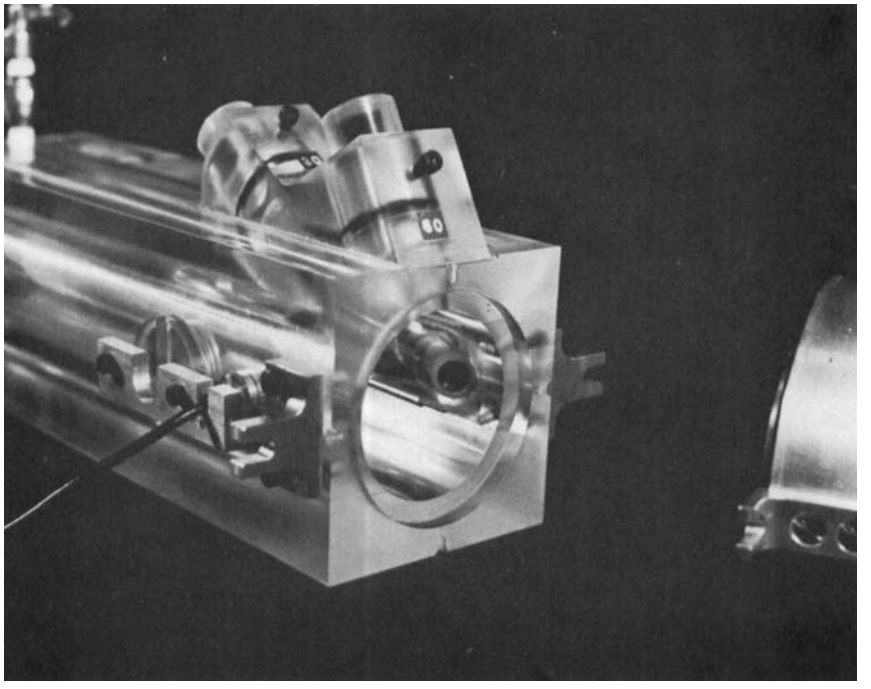

FIGURE 4. The turbulent-flow test-section entrance showing both the hot-film probe and the ultrasonic transducer.

to the other. This delay can be varied to provide the two closely spaced sample volumes used in the ambiguity reduction technique discussed in § 3 of part 1.

The master oscillator frequency used in the experiments was 4·71 MHz. Each burst of this carrier signal applied to the transducer was 1 μs in length, and was repeated with frequencies varying from 7·8 to 15·7 kHz.

The construction of the transducer used in all of the tests, except those § 3.5, is

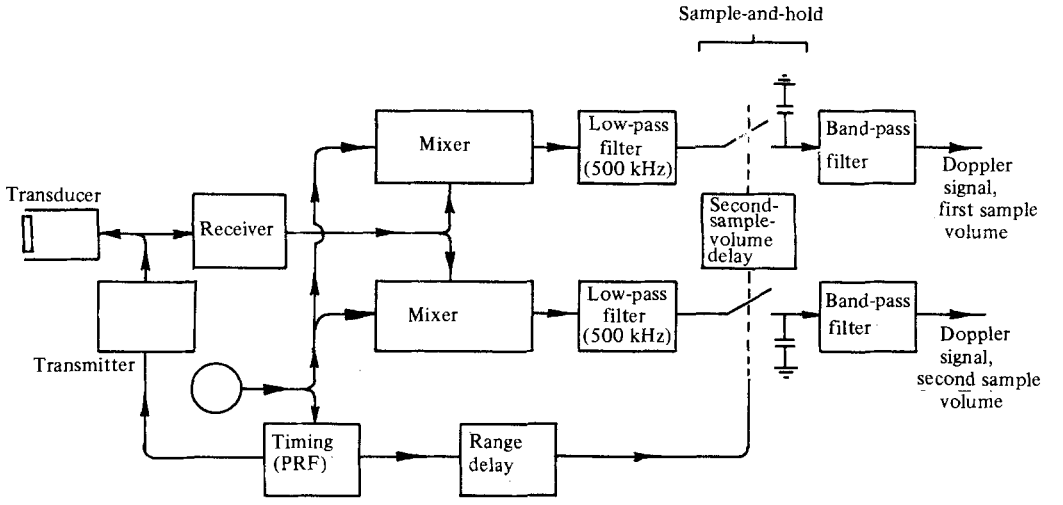

FIGURE 5. A block diagram of the pulsed ultrasonic Doppler velocimeter.

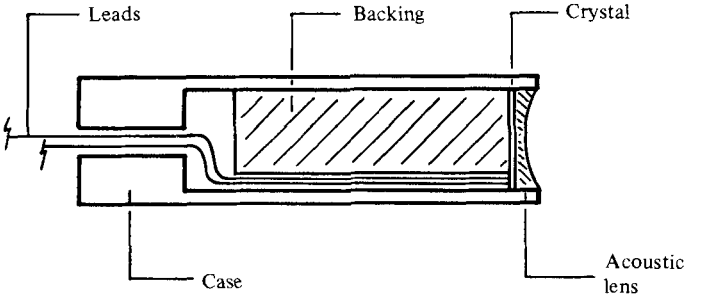

FIGURE 6. Transducer construction.

shown in figure 6. It consisted of a single lead zirconium titanate crystal (commercially known as PZI-5) 0·95 cm in diameter. The damping of the transducer was increased by the addition of backing material composed of a mixture of tungsten powder and epoxy. The resulting quality Q was approximately 8·4. A spherical lens of the same material as the backing was used to focus the acoustic beam and to provide an impedance-matching layer between the crystal and the medium. The focal length of the transducer was 3·25 cm. The focal region, which was more than 1 cm long (measured between the one-half power points along the beam), accommodates both sample volumes with little variation in diameter.

A portion of the experimental procedure required a sample volume large in comparison to the turbulence eddies. To accomplish this, the transducer lens was omitted except for a thin, flat impedance-matching layer, and the backing material was omitted. The lower damping allows the crystal to 'ring' for a longer period after the termination of the driving pulse.

Hot-film anemometer. The thermal-anemometer measurements of the turbulent flow were made with a quartz-coated, conical, hot-film probe (TSI model 1230W). The platinum active element of the probe was 0·012 cm wide by 0·03 cm in diameter.

The signal processing was accomplished with a TSI 1053B bridge anemometer. A TSI model 1310 probe provided temperature compensation.

The working fluid. In both systems a mixture of silicon particles and water was

employed as an acoustic scattering medium for the ultrasonic velocimeter. The silicon particles (GE-antifoam 60) are spherical and non-cohesive. The mean diameter is approximately 5 μm, with standard deviation of 1–2 μm. The volumetric concentration in the mixture employed was approximately 0·02 %.

Clean, degassed water was used for all hot-film measurements. For all measurements, the operating temperature during the experiments was maintained at 20 °C.

3. Single-sample-volume experiments – results and discussion

3.1. *Effective sample-volume directivity*

The effective sample-volume directivity is one of the principal describing parameters of the pulsed ultrasonic Doppler velocimeter, both for laminar and turbulent flow. It enters into the analytical representations of the Doppler signal correlation and the detected velocity signal correlation as the deterministic spatial autocorrelation function $Q(x_1, x_2, x_3)$ ((2.15) and (2.49) in part 1). The directivity appears again as a spatial filter, in § 3 of part 1, in determining the attenuation of the velocity spectrum at high wavenumbers due to finite sample-volume size.

The effective sample-volume directivity is the product of the acoustic-beam directivity and the envelope function of the transmitted bursts. In general, the effective directivity of the sample volume is a three-dimensional function which decreases from the centre continuously in all directions. In assessing the accuracy of the proposed model it was necessary to evaluate this function experimentally. In part 1 expressions for the correlation functions were derived for arbitrary specifications of the three-dimensional sample-volume directivity. In general, the evaluation of expressions containing explicit forms of the sample-volume directivity function is very difficult for turbulent flow and is therefore of limited direct practical value. The Gaussian-shaped sample-volume approximation, discussed in part 1 and repeated here for clarity, allows closed-form evaluation of the modelling equations

$$H(x_1, x_2, x_3) = \text{const.} \times \exp\left\{-\left[\frac{x_1^2}{2\sigma_1^2}+\frac{x_2^2}{2\sigma_2^2}+\frac{x_3^2}{2\sigma_3^2}\right]\right\}. \tag{3.1}$$

If the Gaussian function closely approximates the actual directivity, the results may be applied in a straightforward manner to predict the limitations of measurements in a given flow situation. The Gaussian-shape approximation is defined by the three dimension parameters $\sigma_1, \sigma_2, \sigma_3$. Therefore to apply this model for the directivity, the corresponding widths of the actual sample volume must be determined empirically.

It was shown in part 1 that the spectrum of the Doppler signal is represented by

$$S(\omega) = \text{const.} \times \left\{\exp\left[\frac{-(\omega - k\overline{\langle u_1\rangle}^2}{2\Delta\omega^2}\right] + \exp\left[\frac{-(\omega + k\overline{\langle u_1\rangle})^2}{2\Delta\omega^2}\right]\right\}, \tag{3.2}$$

where

$$\Delta\omega^2 = k^2\Delta\overline{u_1'^2} + \frac{1}{2}\left(\frac{\overline{\langle u_1\rangle}^2}{\sigma_1^2}+\frac{\overline{\langle u_2\rangle}^2}{\sigma_2^2}+\frac{\overline{\langle u_3\rangle}^2}{\sigma_3^2}\right) + k^2\overline{\langle u\rangle_1'^2}.$$

For a focused transducer, the transit-time effect provides a convenient and accurate method of making these measurements. The width of the Doppler signal spectrum in laminar flow is related to the sample-volume dimension by

$$\sigma_s(\theta) = \frac{\overline{U}}{2\pi 2^{\frac{1}{2}}\sigma_v(\theta)}, \tag{3.3}$$

where $\sigma_s(\theta)$ is the spectral deviation (in Hz) of the Doppler signal spectrum, $\sigma_v(\theta)$ is the dimension of the sample volume in the direction of mean velocity which intersects the acoustic beam with Doppler angle equal to θ, and $\bar{U}$ is the mean velocity. Expressing the mean velocity in terms of the mean Doppler frequency $\bar{f}$, the corresponding sample-volume dimension is

$$\sigma_v(\theta) = \frac{\lambda}{4 \times 2^{\frac{1}{2}} \pi \cos\theta \sigma_s(\theta)} \frac{\bar{f}}{}. \tag{3.4}$$

Thus σ_1 equals $\sigma_v(0°)$ and, since the acoustic beam is axisymmetric, σ_2 and σ_3 are equal. Therefore the cross-beam width may be computed from measurements of the axial dimension and the dimension measured at some angle to the beam, $\theta \neq 0°$ (see figure 7) with the use of the relation

$$\sigma_v(90°) = \frac{\sin\theta}{\left[\frac{1}{\sigma_v^2(\theta)} - \frac{\cos^2\theta}{\sigma_v^2(0°)}\right]^{\frac{1}{2}}}. \tag{3.5}$$

An advantage of this method is that it is based on Doppler-shift information. Minor sources of spectral broadening, other than the transit-time effect, associated with the signal processing or the transducer geometry, that are directly proportional to the average velocity will be accounted for in the measured effective sample-volume dimensions. Also, (3.4) indicates that it is not even necessary to know the velocity of the flow or the absolute magnitude of the spectra.

The spectral means and deviations were computed for a variety of velocities in the laminar-flow facility, at Doppler angles of 0° and 45°. The results, shown in figure 8, confirm the implication of (3.4) that the ratio $\bar{f}/\sigma$ of the mean frequency to the spectral deviation is independent of the velocity. In addition, the intersection at the origin of both lines indicates that the only significant spectral broadening effects, in this situation, are directly proportional to velocity. From (3.4) and (3.5), the equivalent sample-volume dimensions for the Gaussian-shape approximation, in this particular trial, are $\sigma_1 = 0{\cdot}049$ cm and $\sigma_2 = 0{\cdot}036$ cm.

To assess the accuracy of the Gaussian-shaped sample-volume assumption a comparison was made between the results of the transit-time tests and a more direct measurement of the actual directivity using echo information. For the cross-beam measurement, a wire target, very small in comparison with the beam width, was positioned incrementally across the beam at the focal-point location of the sample volume. The peak of the resulting echo measured at the output of the receiver was recorded.

Assuming that the acoustic-beam directivity is constant in the axial direction over the length of the sample volume, the effective axial directivity is determined by the modulating envelope function of the transmitted burst. The envelope function was assessed from the time history of a single echo from a target located at the sample volume centre.

Figures 9 and 10 show comparisons of the measured directivities in the axial and cross-beam directions, and the Gaussian-shape approximation based on the dimensions determined by the transit-time method. The amplitudes of these results have been normalized by matching the peak values of the curves. In the cross-beam direction the agreement is excellent. The error in width is of the order of the dimension of the

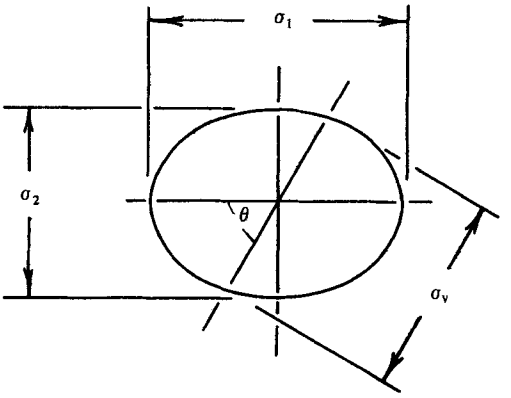

FIGURE 7. Determination of the sample-volume dimensions.

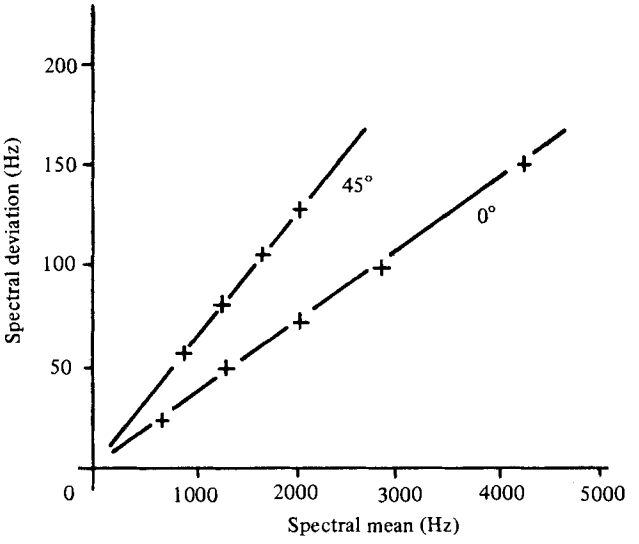

FIGURE 8. Measurement of the spectral deviation *vs.* the spectral mean in laminar flow $\theta = 0°$ and 45°.

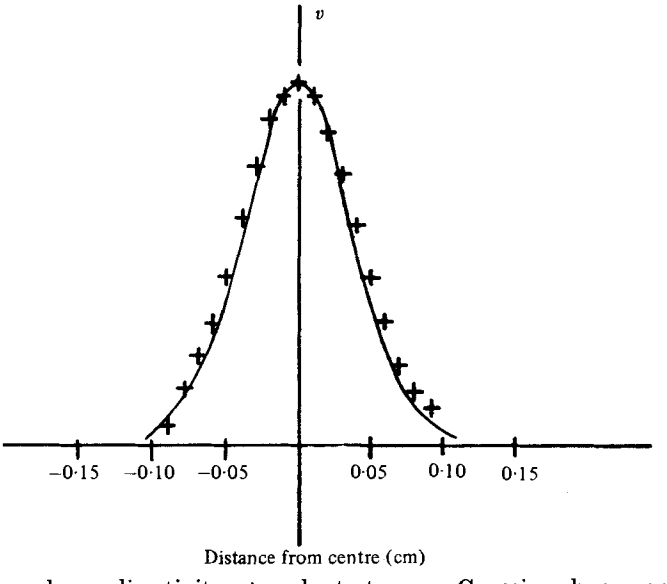

FIGURE 9. Cross-beam directivity. +, echo test; ——, Gaussian-shape approximation.

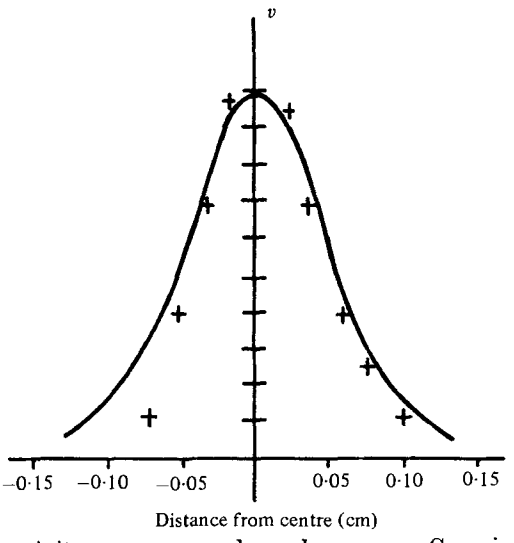

FIGURE 10. Axial directivity. +, measured envelope; ——, Gaussian-shape approximation.

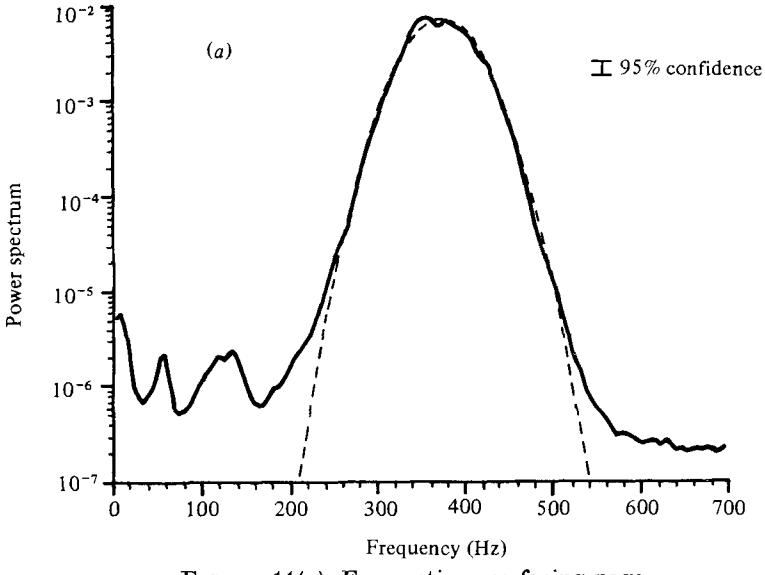

FIGURE 11(a). For caption see facing page.

target used. Axially, the asymmetry of the rise and decay of the transmitted burst, particularly at the start of the excitation, causes a more significant deviation from the Gaussian approximation. However, the two shapes are at least qualitatively consistent, and the width parameters are nearly identical.

A further evaluation of the approximation may be made by examining the shape of the Doppler signal spectrum. For the Gaussian-shaped sample-volume approximation, the form of the Doppler spectrum is given by (3.2). This equation is the basis for the transit-time measurement of the sample volume width just described. With this width substituted back into the equation, a comparison can be made with the measured spectral estimate. Figure 11 (*a*) is characteristic of such a comparison for laminar flow.

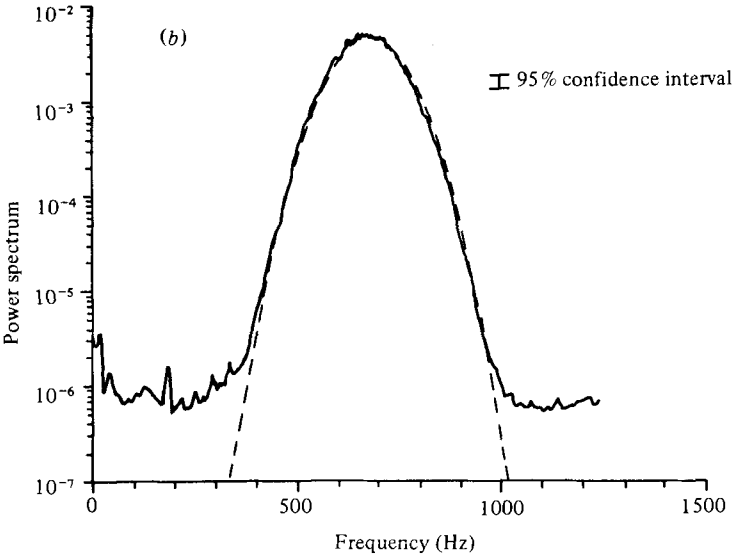

FIGURE 11. Measured (——) and theoretical (– – –) spectra in (*a*) laminar and (*b*) turbulent flow.

The spectral amplitudes have been normalized by the peak values. Figure 11(*b*) shows a typical corresponding result for turbulent flow. Both results show close agreement between the theoretical and experimental spectral shape to three or four orders of magnitude below the peak values.

The results suggest that the Gaussian-shape assumption is an adequate representation of the effective directivity for a high-resolution Doppler velocimeter within the restrictions of the model. In addition, the results indicate that the laminar flow, transit-time method of determining the dimensions of the sample volume is accurate, as well as convenient.

3.2. *The detected velocity signal spectrum – laminar flow*

The detected velocity signal is defined as the instantaneous time-rate of change of phase of the Doppler signal. In § 2.2 of part 1, it was shown that the detected velocity consists of the spatial average of the velocities within the sample volume plus the Doppler ambiguity process. In the design of any measurement of turbulence with the pulsed Doppler velocimeter it is essential to be able to predict the magnitude of the unwanted ambiguity process. Theoretically, the power spectrum of the ambiguity, assuming the Gaussian-shaped sample-volume approximation to be valid, is given by

$$\left.\begin{aligned} S_{\dot{\Phi}}(\omega) &= \tfrac{1}{2}\pi^{\frac{1}{2}}\Delta \sum_{n=1}^{\infty} n^{-\frac{3}{2}} \exp\left[-\frac{\omega^2}{4n\Delta^2}\right], \\ \Delta^2 &= \frac{1}{2}\left(\frac{\overline{\langle u_1\rangle^2}}{\sigma_1^2}+\frac{\overline{\langle u_2\rangle^2}}{\sigma_2^2}+\frac{\overline{\langle u_3\rangle^2}}{\sigma_3^2}\right)+k^2\overline{\Delta u'^2}. \end{aligned}\right\} \tag{3.6}$$

The accuracy of this result was explored experimentally in the laminar-flow facility. In the absence of the turbulent-velocity fluctuations the ambiguity process is isolated in the measurement of the detected velocity signal spectrum.

The measured power spectra of the detected velocity signal for various velocities,

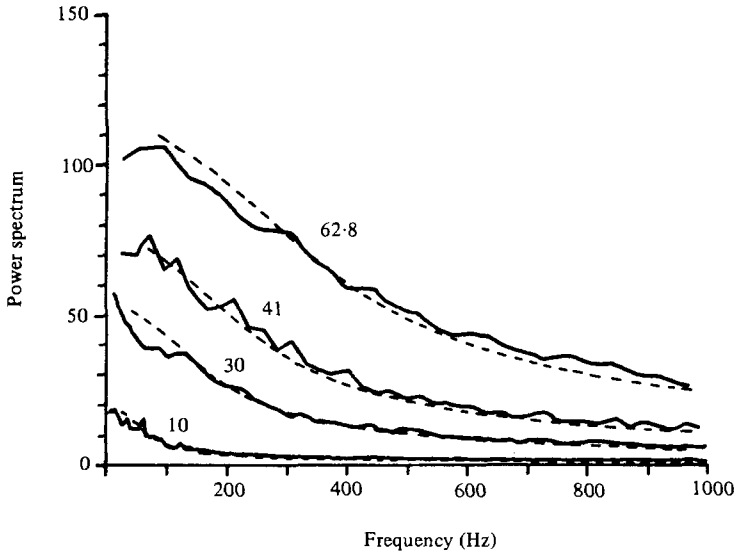

FIGURE 12. Detected velocity spectrum in laminar flow showing the effect of transit time on the ambiguity process. ——, ultrasonic velocimeter; – – –, theoretical. Mean velocity: 62·8, 41, 30, 10 cm/s; $\theta = 60°$. The spectral estimates are based on averages of 200 records of 512 points each.

and with the Doppler angle equal to 60° are plotted in figure 12 and are compared with the model. In all cases, the mean value of the detected velocity signal, which corresponds to the actual velocity, has been subtracted before calculation of the spectra. The theoretical predictions of these spectra are computed from (3.6), the Euler–Maclaurin sum formula was used to improve the rate of convergence. The sample-volume dimensions were determined by the transit-time method described in § 3.1.

In addition to confirming the theoretical results, figure 12 also shows the relationship of the velocity-ambiguity process and the transit-time effects. As the velocity increases, the transit time decreases and the ambiguity spectrum increases in both magnitude and bandwidth. This might be interpreted as an increase in the uncertainty of the velocity as the time that an individual particle spends in the measuring volume is decreased.

3.3. *Doppler velocimeter measurements of intensities and turbulence spectra*

Measurements of the axial-velocity fluctuations in the core region of fully developed pipe flow were made by means of hot-film anemometry. These data provide the basis for comparison of the pulsed ultrasonic velocimeter results to those of an instrument of established reliability. Comparisons with the ultrasonic velocimeter were made primarily on the basis of velocity spectrum and turbulence intensity.

The range of Reynolds numbers (based on the diameter and the local mean velocity) extends from 6000 to 40 000. The corresponding range of turbulence intensities extends from 4·4 % at a Reynolds number of 6000 to 3·7 % at 40 000.

Figure 13 shows the hot-film measurements of the velocity-fluctuation spectra. The abscissa is normalized according to the dimensionless Strouhal number kD, where k is the wavenumber and D is the tube diameter. The ordinate is $E_{\mathrm{L}}(k)/\overline{u'^2}D$,

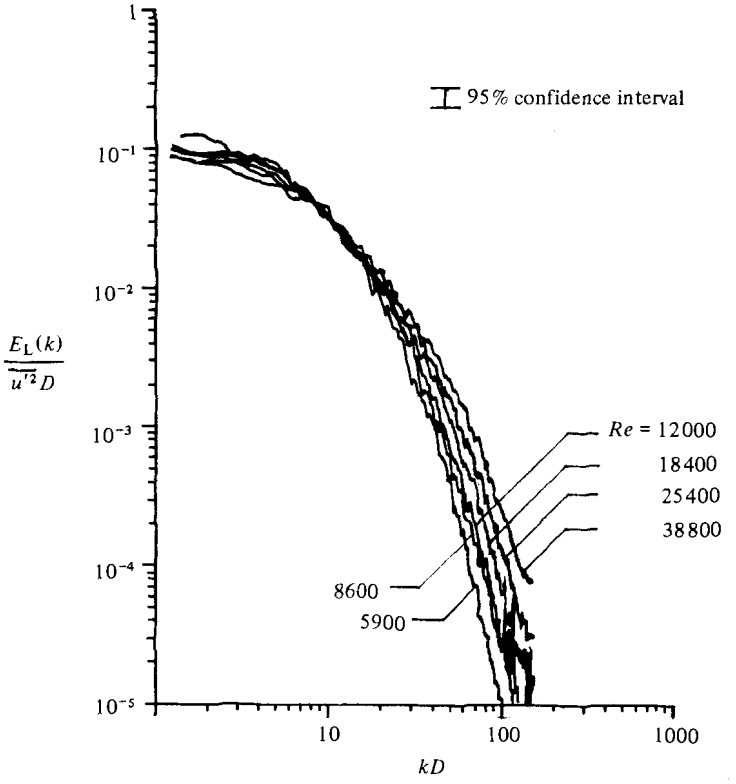

FIGURE 13. Hot-film-anemometer measurement of turbulence spectrum.

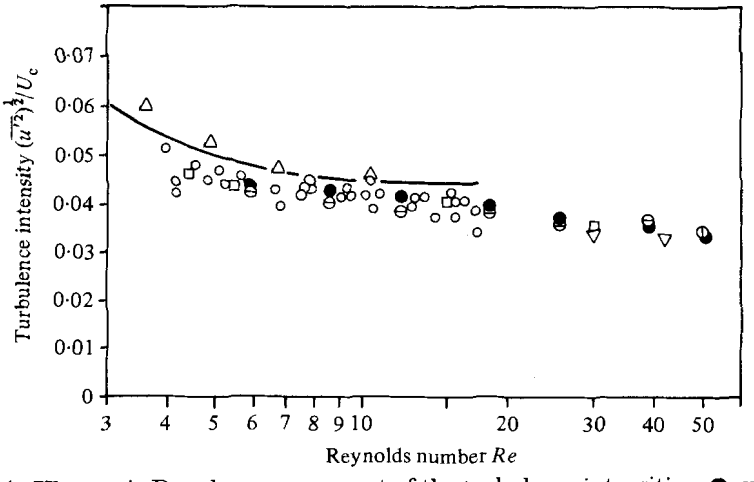

FIGURE 14. Ultrasonic Doppler measurement of the turbulence intensities. ●, ultrasonic velocimeter, $\theta = 45°$; ⊖, hot-film anemometer; ——, Bourke *et al.* (1968) (hot-wire); ○, Goldstein & Kried (1968) (laser); ⓘ, Laufer (1954) (hot-wire); □, Pennell, Sparrow & Eckert (1972) (hot-film); △, Pike, Jackson & Page (1968) (laser); ▽, Resch & Coantic (1969) (hot-film).

where $E_L(k)$ is the one-dimensional longitudinal energy spectrum and $\overline{u'^2}$ is the mean-square value of the velocity fluctuations.

The spectra are in close agreement with other published experimental results (Resch & Coantic 1969; Lawn 1971). In the following sections these measurements

are assumed to be correct representations of the velocity fluctuations. The data are used both for comparison and as a basis for theoretical predictions of the ultrasonic velocimeter output.

Turbulent-flow velocity measurements were made with the pulsed ultrasonic Doppler velocimeter. The ultrasonic determinations of the turbulence intensity were inferred from the Doppler spectrum using (2.14) for a Doppler angle of 45°.

The ultrasonic results along with the hot-film measurements made as part of this investigation are shown in figure 14. The hot-film intensity estimates were computed from the integral of the velocity spectra. Also plotted are a number of published results of pipe-flow investigations that employed both thermal and laser–Doppler anemometry in water, as well as in air and in carbon dioxide. Over the range of Reynolds numbers shown, the ultrasonic measurements are within expected experimental error of the hot-film measurements.

In evaluating the one-dimensional turbulence spectrum with the ultrasonic velocimeter the two most significant considerations are the level of the Doppler-ambiguity process and the attenuation of the spectrum caused by spatial averaging of the velocities within the sample volume. The corresponding relations for isotropic, low-intensity, turbulent flow were developed in part 1 and are restated here in a form convenient for this discussion. The spectrum of the detected velocity signal

$$S_{\omega_{\mathrm{d}}}(\omega) = S_{\langle u_1\rangle}(\omega) + S_{\dot{\Phi}}(\omega), \tag{3.7}$$

where

$$S_{\langle u_1\rangle}(\omega) = \frac{\pi}{\overline{U}_1}[\langle E_{\mathrm{L}}(k_1)\rangle \cos^2\theta + \langle E_{\mathrm{T}}(k_1)\rangle \sin^2\theta] \tag{3.8}$$

is the spectrum of the spatially averaged velocity fluctuations; θ is the Doppler angle, $\overline{U}_1$ is the mean velocity, $\langle E_{\mathrm{L}}(k_1)\rangle$ and $\langle E_{\mathrm{T}}(k_1)\rangle$ are respectively the longitudinal and transverse spectra of the spatially averaged velocity fluctuations, and the wave vector k_1 is related to the radian frequency ω by $k_1 = \omega/\overline{U}_1$. The spectra of the spatially averaged velocity fluctuations are related to the actual longitudinal velocity spectrum and the sample volume directivity by

$$\langle E_{\mathrm{L}}(k_1)\rangle = \exp(-\sigma_1^2 k_1^2)\, E_{\mathrm{L}}(k_1) + 2\sigma_2^4 \exp[-k_1^2(\sigma_1^2-\sigma_2^2)] \times \int_{k_1}^{\infty} \exp(-\sigma_2^2\xi^2)(\xi^2 - k_1^2 - 2/\sigma_1^2)\, E_{\mathrm{L}}(\xi)\, d\xi, \tag{3.9}$$

$$\langle E_{\mathrm{T}}(k_2)\rangle = -\tfrac{1}{2}\exp(-\sigma_2^2 k_2^2)\left\{k_2\frac{d}{dk_2}[E_{\mathrm{L}}(k_2)] + E_{\mathrm{L}}(k_2)[k_2^2(\sigma_1^2+\sigma_2^2) - 1] - \frac{2}{\pi}\int_{k_2}^{\infty} F[(\xi^2 - k_2^2)^{\frac{1}{2}}]\, E_{\mathrm{L}}(\xi)\, d\xi\right\}, \tag{3.10}$$

where

$$F(\rho) = 2\int_0^{\pi} e^{-\rho^2\gamma}[\gamma(\gamma k^2 - 2\sin^2\theta) + \rho^2\gamma^2\sin^2\theta]\, d\theta,$$

$$\gamma = \sigma_1^2\cos^2\theta + \sigma_2^2\sin^2\theta.$$

Since, at a given frequency, the Doppler ambiguity artificially raises the value of the spectrum while the spatial averaging tends to decrease it, a single experiment in which both effects are included to a comparable degree would not be conclusive.

Therefore in this section results are presented for which the sample volume is small with respect to the turbulence scale. The effect of spatial attenuation of the spectrum is far less significant than that of the ambiguity process. In § 3.4 the consequences of using a large sample volume for spectral measurements are explored.

For a given-size sample volume the spatial attenuation of the one-dimensional velocity spectrum increases with the Reynolds number. To demonstrate that the spatial attenuation is small, consider the case of the Reynolds number equal to 38800 and a spherically symmetric sample volume 0·05 cm in diameter. The hot-film measurement of the longitudinal velocity spectrum is plotted in figure 15, accompanied by the theoretical prediction of the spectrum of the spatial average velocity given by (3.9). Over the frequency range shown, the attenuation is small. Since all of the following data were collected in flows for which the Reynolds number is below 38800 the attenuation of the spectrum is even less.

The results of the ultrasonic measurements are normalized for comparison with the hot-film anemometer data. If $S_D(\omega)$ is the power spectrum of the detected velocity signal, with units of $(\text{rad/s})^2/(\text{rad/s})$, then the corresponding normalization is

$$\frac{E_\theta(k)}{\overline{u'^2}D} = \frac{S_D(\omega)\,\overline{U}}{\pi k_D^2 \overline{u'^2} D}, \tag{3.11}$$

where $\overline{U}$ is the local mean velocity, k_D is the magnitude of the ultrasonic wave vector ($k_D = 2\omega_0/c$), $\overline{u'^2}$ is the mean-square value of the velocity fluctuations, D is the pipe diameter, and $E_\theta(k)$ is the one-dimensional turbulence spectrum.

The results for the range of Reynolds numbers from 6000 to 40000 are shown in figure 16. Each graph includes ultrasonic measurement of the turbulence spectrum and the corresponding hot-film measurement. The hot-film measurements have been corrected to correspond to the proper Doppler angle according to the isotropic relationship given by (3.8).

In all cases, the ultrasonic measurement follows that of the hot-film anemometer closely until the level of the spectrum of the ambiguity process is reached. For all flow rates, these ultrasonic measurements are limited to the first order of magnitude of the spectrum compared with four or more for the hot-film anemometer. For the chosen normalization, the velocity spectrum at the centre of the pipe for fully developed turbulent flow is *approximately* invariant with respect to changes in diameter and flow rate. The amplitude of the ambiguity spectrum (transit-time effect only) at the origin is

$$\frac{S_{\dot{\Phi}}(0)\,\overline{U}}{\pi k_D^2 \overline{u'^2} D} = \frac{2{\cdot}3}{2^{\frac{1}{2}}\pi\sigma_v D k_D^2 (\overline{u'^2}/\overline{U}^2)}. \tag{3.12}$$

Since the variation of the turbulence intensity with Reynolds number is relatively small, the ambiguity level can only be lowered by increasing the acoustic carrier frequency or the size of the sample volume. It has been shown that the sample-volume size cannot be increased indefinitely without causing significant distortion of the velocity spectrum. In addition, acoustic attenuation places practical limits on the carrier frequency. Notice that the relative amplitude of the ambiguity would be even greater for a smaller diameter pipe.

The accuracy of the model of the pulsed Doppler velocimeter in turbulence may also be assessed by comparing the theoretical detected velocity signal spectra, based on

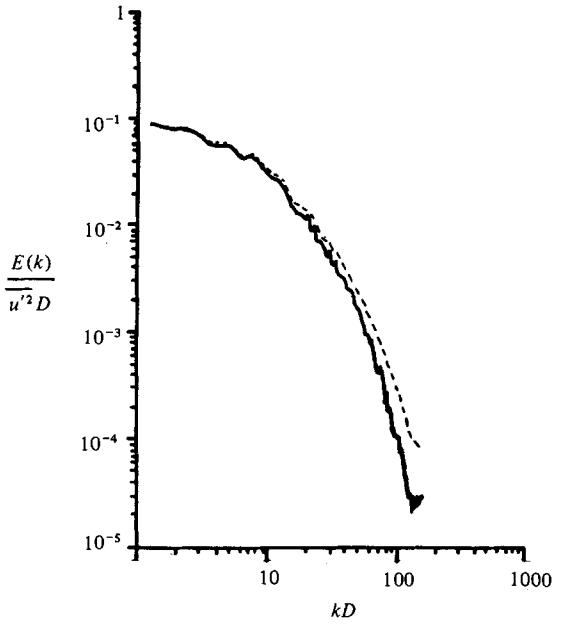

FIGURE 15. Theoretical effect of spatial averaging on the spectrum for a relatively small sample volume. – – –, longitudinal spectrum; ——, theoretical spatial average; Re = 38800.

the hot-film anemometer data used in (3.6)–(3.10), with the corresponding ultrasonic measurements. The comparisons for the Reynolds number range from 6000 to 40000 are shown in figure 17. Although the effect of spatial averaging of the spectra is small, it has been included in all of these calculations.

Generally, these results indicate that the ultrasonic Doppler velocimeter is capable of accurate measurement of velocity fluctuations within the restrictions imposed by the ambiguity process. In addition, they confirm the theoretical prediction of the Doppler ambiguity in turbulent flow as well as its statistical independence from the velocity fluctuations.

From (3.6), two phenomena contribute substantially to the level of the ambiguity spectrum: (i) the transit-time effect (also present in laminar flow), and (ii) the turbulence-induced deviations of the velocity within the sample volume from the spatial average velocity. It is interesting to note the relative contributions of these two terms in the situations investigated. The mean-square velocity deviation $\overline{\Delta u'^2}$ is equal to the integral of the difference between the actual velocity spectrum and the spectrum of the spatial average velocity. That is

$$\overline{\Delta u'^2} = \int_{-\infty}^{+\infty} [E_1(k_1) - \langle E_1(k_1)\rangle]\, dk_1.$$

Since it is proportional to both the magnitude and width of the ambiguity spectrum, the parameter Δ^2 of (3.6) may be taken to be a measure of the ambiguity. Then the portion of the ambiguity caused by the transit-time effects is

$$\frac{1}{2}\left(\frac{\overline{\langle u_1\rangle^2}}{\sigma_1^2} + \frac{\overline{\langle u_2\rangle^2}}{\sigma_2^2} + \frac{\overline{\langle u_3\rangle^2}}{\sigma_3^2}\right),$$

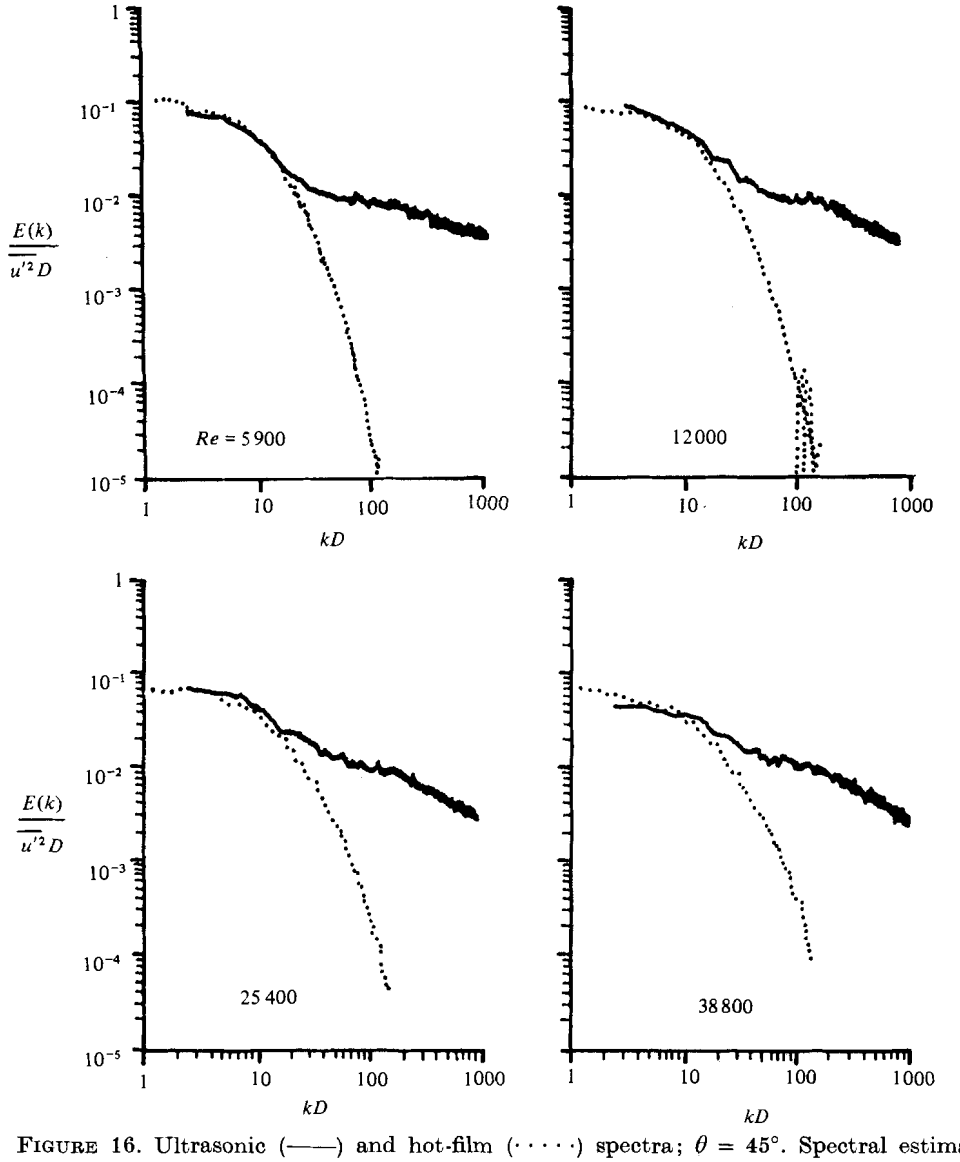

FIGURE 16. Ultrasonic (——) and hot-film (· · · · ·) spectra; $\theta = 45°$. Spectral estimates for ultrasonic measurements are based on an average of 100 data records of 2048 points/record with frequency smoothing (Hanning).

while that resulting from turbulence effects is $k^2\overline{\Delta u'^2}$. The theoretical contribution of the turbulence-induced ambiguity for the Reynolds numbers at which data were collected is shown as a percentage of the total in figure 18. The trend shows that, as the mean velocity is increased, the mean-square value of the velocity deviations increases faster than the transit-time effect.

Over the range considered here this effect is a relatively small part (maximum of 3·5 %) of the total ambiguity. Of course, this would be true in any properly designed turbulence-spectrum measurement. That is, the size of the sample volume should be sufficiently small to avoid large spatial averaging of the spectrum. This implies that,

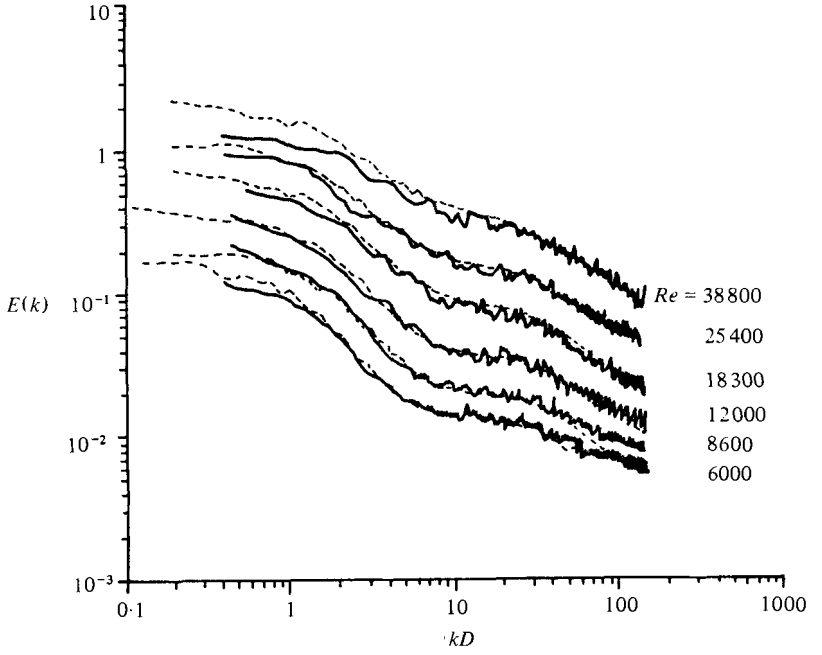

FIGURE 17. Comparison of the analytical model with the spectrum of the detected velocity for turbulent flow; $\theta = 45°$. – – –, theoretical; ——, ultrasonic. Spectral estimates for ultrasonic measurements are based on an average of 100 data records of 2048 points/record with frequency smoothing (Hanning).

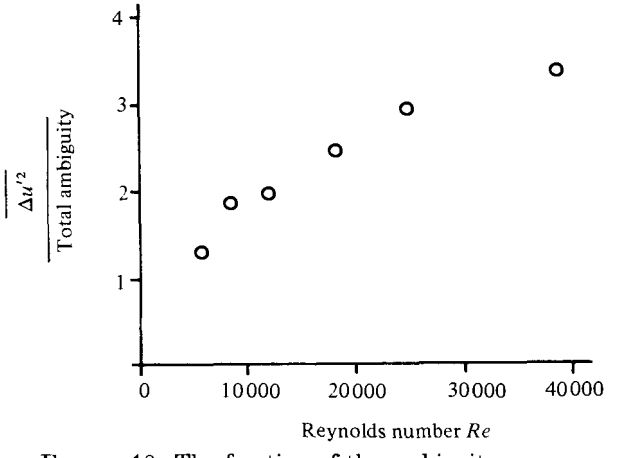

FIGURE 18. The fraction of the ambiguity process caused by velocity variations within the sample volume.

when these conditions apply, the ambiguity spectrum for turbulent flow can be estimated accurately on the basis of the transit time alone. Since the velocity fluctuations and the Doppler ambiguity are independent random processes, an improved estimate of the velocity spectrum can be obtained by subtracting the predicted ambiguity spectrum from the measured spectrum.

This technique has been used in laser anemometry, where it has been shown (George & Lumley 1973) that, in many instances, the corresponding ambiguity spectrum is

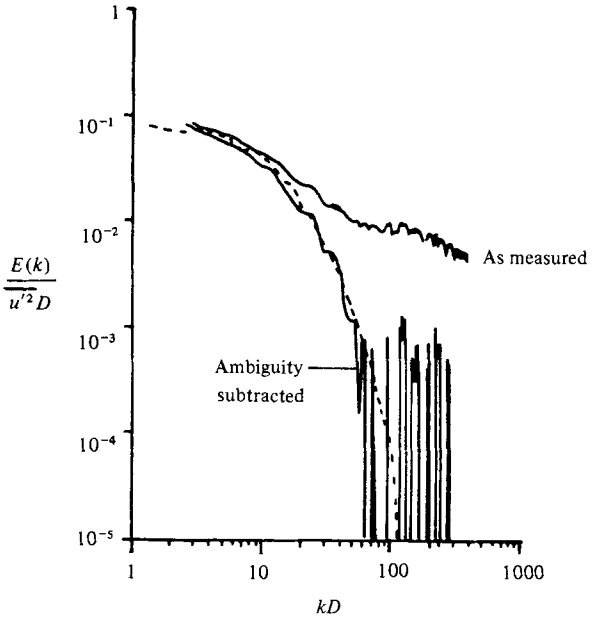

FIGURE 19. Improvement of the turbulence-spectrum measurement by subtracting the theoretical ambiguity spectrum. ——, ultrasonic velocimeter; – – –, hot-film; Re = 12000, θ = 45°. Spectral estimates for ultrasonic measurements are based on an average of 100 data records of 2048 points/record with frequency smoothing (Hanning).

nearly constant over the entire range of significant frequencies. In that case it is sufficient to subtract an easily computed constant from each component of the measured spectrum. Unfortunately, this is not generally true for the ultrasonic Doppler velocimeter. The ambiguity spectrum diminishes appreciably across the range of the velocity spectrum. Therefore it is necessary to compute the ambiguity spectrum at each frequency component. An example of this method is shown in figure 19. The improvement, measured as the ratio of the powers at which the corrected and uncorrected spectra deviate radically from the actual spectrum, is more than one order of magnitude. This graph also illustrates the limiting factors in the technique. The theoretical prediction of the ambiguity deviates from the corresponding portion of the measured spectrum in two ways. First, the theory is only an approximation of the actual ambiguity process. Secondly, the measured spectrum is subject to statistical estimation errors. The latter restriction may be overcome, at the expense of increased data-collection and processing time, by reducing the variance and bias of the spectral estimate. Furthermore, in § 3.2, the theoretical ambiguity spectrum agrees with the experimental measurement with an error on the order of 5–10 %. Therefore the improvement in the velocity spectrum measurement achieved by subtracting the theoretical ambiguity spectrum is probably limited to less than two orders of magnitude.

3.4. *Large-sample-volume measurements*

As the size of the sample volume is reduced, the amount of attenuation of the velocity spectrum caused by spatial averaging decreases. Simultaneously, the transit-time effect accounts for an increasing share of the ambiguity spectrum (first term for the expression for Δ^2 in (3.6)). In § 3.3 a small sample volume was employed to investigate

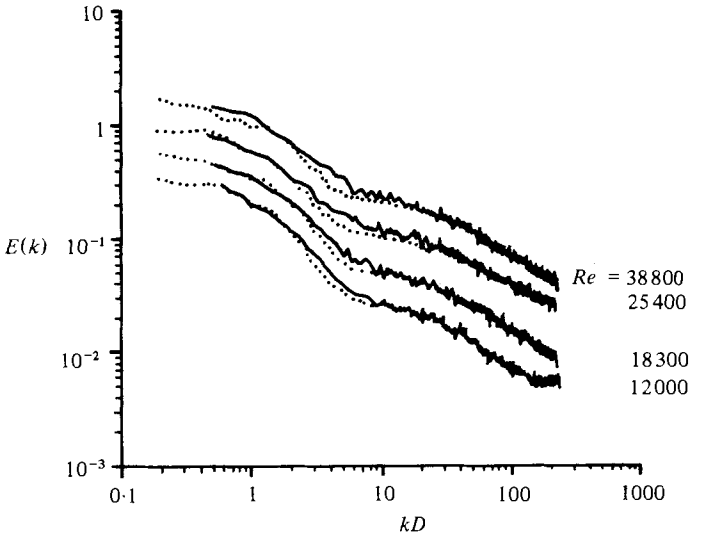

FIGURE 20. Large-sample-volume turbulence-spectrum measurement. ——, ultrasonic; · · · · ·, theoretical, based on hot-film; $\theta = 45°$. Spectral estimates for ultrasonic measurements are based on an average of 200 data records of 2048 points/record with frequency smoothing (Hanning).

the characteristics of the model when these trends are dominant. In this section a much larger sample volume is used to examine the accuracy of the analysis in situations where the effects of spatial averaging on the spectrum are large and where turbulence-induced variations in velocity within the sample volume (sceond term in the expression for Δ^2 in (3.6)) contribute significantly to the total ambiguity. Under some circumstances, it may be impracticable to employ a sample volume that is small relative to the scale of turbulence. Therefore knowledge of the degree to which a given measurement is corrupted is fundamental.

The velocity-spectrum measurements were made for Reynolds numbers of 12000, 18300, 25400 and 38800. The sample volume was produced with a transducer consisting of a piezoelectric crystal that was unfocused, air-backed and 0·35 cm in diameter. The characteristic dimensions of the sample volume, determined by the echo method described earlier, were $\sigma_1 = 0{\cdot}07$ cm in the axial direction and $\sigma_2 = 0{\cdot}17$ cm in the cross-beam direction.

The velocity spectra, as measured with the ultrasonic velocimeter, are shown in figure 20. As expected, the spectral components related to the random-velocity process are only discernible until the level of the wide-band Doppler ambiguity process is encountered. The theoretical predictions, also shown, are the sum of the spatially averaged spectrum (3.8) and the ambiguity spectrum (3.6). They are based on the actual spectrum obtained with the hot-film anemometer.

In all cases shown, the amount of ambiguity caused by the velocity variations within the sample volume is theoretically greater than 53 % of the total. These results combined with those of § 3.3, where the corresponding value is less than 3·5 %, confirm the validity of the analysis of the Doppler-ambiguity process caused by *both* transit-time effect and turbulence-induced spatial velocity variations.

In figure 21 the ambiguity spectrum has been subtracted from each experimental

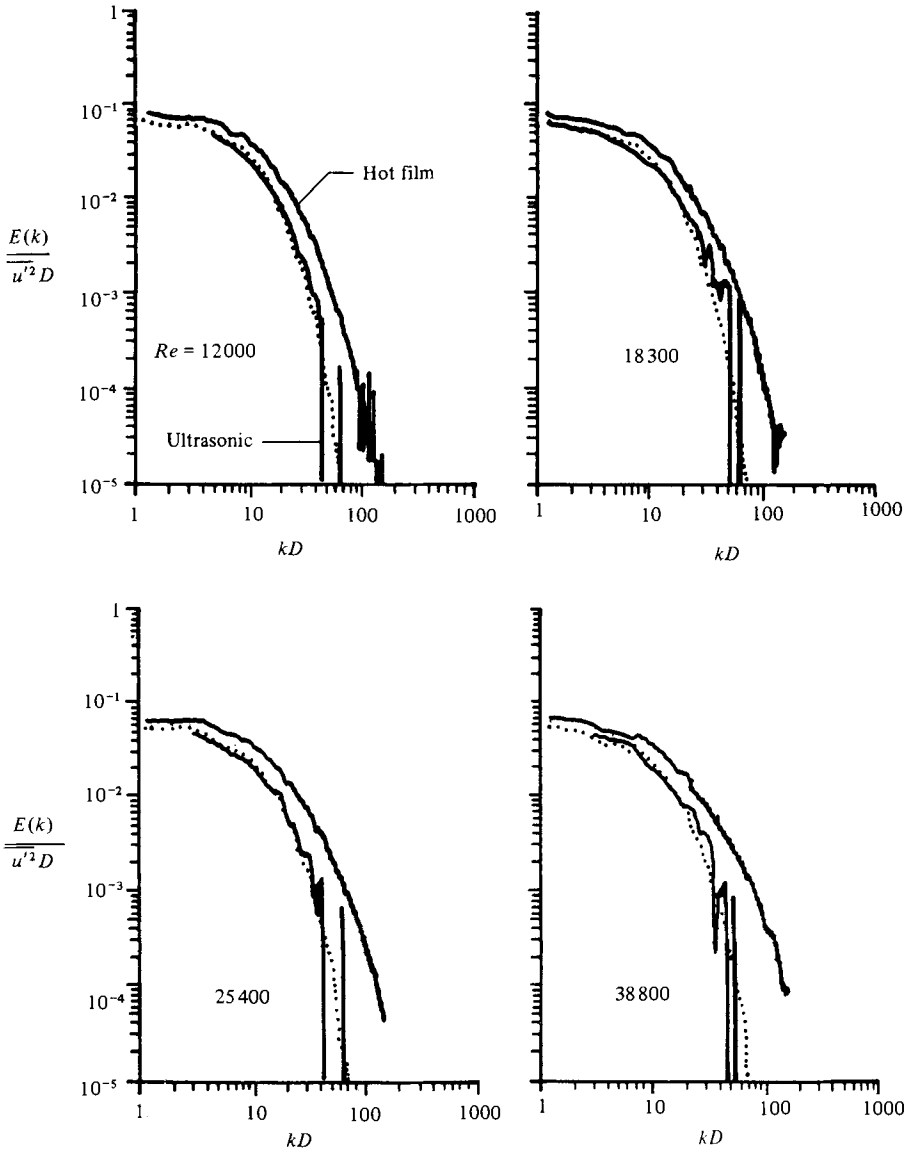

FIGURE 21. The effect of spatial averaging; $\theta = 45°$. · · · · ·, theoretical spatial average.

result to illustrate the attenuation of the velocity spectrum resulting from spatial averaging of the velocity in the sample volume. Also shown are the corresponding hot-film velocity spectrum and the theoretical spectrum of the spatial average of the velocity, (3.8). The agreement between the analysis and the experimental results is good, but deteriorates at lower spectral amplitudes owing to the large variance of the ambiguity components of the spectrum.

Another possible source of error in this series of experiments is the assumption of a Gaussian-shaped volume. The actual sample volume produced with the unfocused transducer and long driving burst duration deviates farther from the Gaussian function than does that of the small, highly focused transducer employed in § 3.3.

4. Dual-sample-volume techniques – results and discussion

4.1. *Dual-sample-volume ambiguity-reduction technique – laminar flow*

In part 1 the theoretical aspects of the reduction of the Doppler ambiguity in the measurement of the velocity spectra by the dual-sample-volume method were examined. Using this technique, the velocity spectrum is estimated by computing the cross-spectrum of the detected velocity signals from two closely spaced sample volumes. The results of § 3.3 indicated that the accuracy of the velocity spectrum estimate can also be improved by subtracting the theoretical prediction of the ambiguity spectrum from the measured spectrum. The principal advantage of the dual-sample-volume method is that it does not depend directly on, and therefore is not limited by, the accuracy of an analytical result. The ambiguity is removed by virtue of independence of the particle populations of the two spatially separated sample volumes.

There are two disadvantages of the dual-sample-volume method. First, it requires additional data processing to compute the cross-spectrum. Secondly, distortion of the spectrum at high wavenumbers can result if the sample volumes are placed too far apart. However, substantial decreases in the level of the Doppler-ambiguity spectrum are possible with only small separations.

In part 1 it was shown that the cross-spectrum of the detected velocity signals from two sample volumes is equal to

$$S_{\omega_\alpha \omega_\beta}(\omega) = S_{\langle u_1\rangle_\alpha \langle u_1\rangle_\beta}(\omega) + S_{\alpha\beta}(\omega), \tag{4.1}$$

where $S_{\langle u_1\rangle_\alpha \langle u_1\rangle_\beta}(\omega)$ is approximately equal to the one-dimensional velocity spectrum and $S_{\alpha\beta}(\omega)$ is the spectrum of the remaining Doppler ambiguity. The term $S_{\langle u_1\rangle_\alpha \langle u_1\rangle_\beta}(\omega)$ is related to the actual velocity spectrum by the Fourier transform of the correlation function

$$\begin{aligned} P_{11}(x) = {} & f((x^2 + \nu_1^2 \sin^2\theta_D))^{\frac{1}{2}} \cos^2\left[\theta_D - \arctan\frac{\nu_1 \sin\theta_D}{x}\right] \\ & + g((x^2 + \nu_1^2 \sin\theta_D)^{\frac{1}{2}}) \sin^2\left[\theta_D - \arctan\frac{\nu_1 \sin\theta_D}{x}\right], \end{aligned} \tag{4.2}$$

where $f(r)$ and $g(r)$ are the actual longitudinal and transverse correlation functions, x is the apparent separation (Taylor's hypothesis) of the sample volumes in the direction of the mean flow, θ_D is the Doppler angle, and ν_1 is the distance of separation of the sample volumes along the axis of the acoustic beam. Further, the spectrum of the remaining Doppler ambiguity is given by

$$S_{\alpha\beta}(\omega) = \tfrac{1}{2}\pi^{\frac{1}{2}} u \exp\left[-i\frac{\omega v}{u^2}\right] \sum_{n=1}^{\infty} \exp[-2nw]\, n^{-\frac{3}{2}} \exp\left[\frac{-(\omega^2 - 4n^2v^2)}{4nu^2}\right], \tag{4.3}$$

where

$$u^2 = k^2\overline{\Delta u'^2} + \frac{\overline{\langle u_1\rangle^2}}{2\sigma_1^2} + \frac{\overline{\langle u_2\rangle^2}}{2\sigma_2^2} + \frac{\overline{\langle u_3\rangle^2}}{2\sigma_3^2},$$

$$v = \frac{\overline{\langle u_1\rangle}\,\nu_1}{2\sigma_1^2}, \quad w = \frac{\nu_1^2}{4\sigma_1^2}.$$

To demonstrate the effectiveness of this method and to verify the theoretical

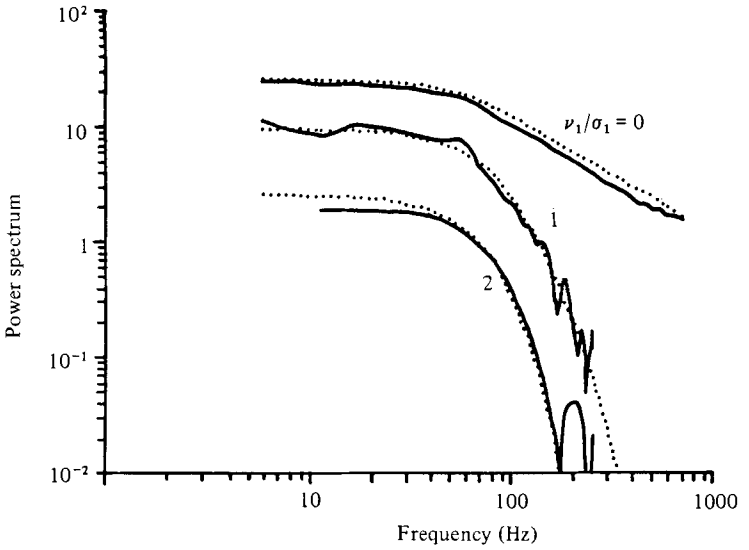

FIGURE 22. Ambiguity spectrum reduction resulting from spatial separation of the sample volumes. ——, ultrasonic; · · · · ·, theoretical; $\theta = 60°$. Spectral estimates for ultrasonic measurements are based on an average of 2000 data records for 256 points/record with frequency smoothing (Hanning).

analysis, a series of tests was performed in the laminar-flow facility. The cross-spectra of the detected velocity signals from two sample volumes were computed. The cross-spectral magnitude for various sample volume separations and with the Doppler angle equal to 60° are shown in figure 22. The separation of the sample volumes ν is normalized by the characteristic dimension σ_1 in the axial direction. Since no turbulent-velocity fluctuations are present, these spectra represent only that portion of the ambiguity process which remains correlated. These measurements illustrate the effect of overlap of the sample volumes. The measured cross-spectrum of the detected velocities from two completely overlapping sample volumes is virtually identical with the auto-spectrum for a single-sample-volume measurement. Note that the ambiguity spectrum is greatly reduced in both magnitude and bandwidth for moderate separations of the sample volumes. The theoretical magnitude of the corresponding ambiguity spectra accompany each measured result. The agreement is clearly adequate to confirm the previous analysis.

The effect of the variation of the Doppler angle was also investigated empirically. The acoustic beam was positioned at angles of 0° and 20° with respect to the direction of the mean flow. The sample volumes were widely separated ($\nu/\sigma_1 = 4$). The measured cross-spectra of the ambiguity processes for these cases, as well as the auto-spectrum for a single sample volume, are shown in figure 23. For the situation in which the Doppler angle is equal to zero, the level of the ambiguity is nearly as great as the auto-spectrum, even though the overlap of the sample volumes is minimal. Theoretically, if the particle populations passed without relative motion from the upstream sample volume to the one behind, the two processes would differ only by the delay time $\nu/\overline{U}$. The magnitude of the cross-spectrum would be identical with that of the auto-spectrum. The measurement indicates that although the processes were highly correlated, some attenuation does occur for very large separations. (Note the linear scale on

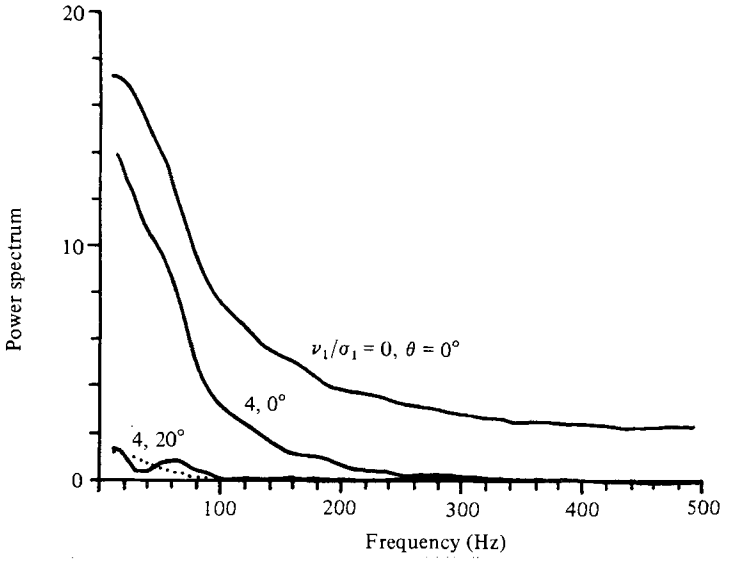

FIGURE 23. The effect of 'shadowing' on the reduced ambiguity spectrum. ——, ultrasonic; · · · · ·, theoretical. Spectral estimates for ultrasonic measurements are based on 2000 data records of 256 points/record with frequency smoothing (Hanning).

the ordinate.) This attenuation may have been caused by small motions of the particles during the transition, from one sample volume to the other.

The result for the same separation but with the Doppler angle equal to 20°, also in figure 23, shows that as the downstream sample volume is removed from the shadow of the other, the correlation between the ambiguity processes is greatly reduced. The corresponding theoretical ambiguity magnitude is also shown.

The outcome of these laminar-flow measurements confirm the dependence of the Doppler-ambiguity process on the particle populations of the individual sample volumes. In addition, the model of the cross-spectral magnitude of the ambiguity process for the dual-sample-volume method appears to be accurate in the cases investigated.

4.2. *Dual-sample-volume ambiguity-reduction techniques – turbulent flow*

The useful dynamic range of the pulsed Doppler velocimeter in measuring one-dimensional velocity spectra in turbulent flow can be extended by use of the dual-sample-volume method of reducing the masking effects of the Doppler ambiguity spectrum. To demonstrate the feasibility of this technique, measurements of the cross-spectral density of the detected velocity signals from two sample volumes in the turbulent pipe-flow system were made. To avoid excessive attenuation of the spectra at high wavenumbers caused by spatial averaging of the velocity fluctuations, the small sample volume ($\sigma_1 = 0{\cdot}05$ cm, $\sigma_2 = 0{\cdot}036$ cm) was employed. Results were obtained for Reynolds numbers of 12000 and 25400. For each Reynolds number measurements were made using two Doppler angles: 45° and 60°. In each case, the cross-spectra were measured for separations ν of the sample volumes equal to $\nu/\sigma_1 = 0, 1, 2$ and 3. The results are presented in figure 24, along with the corresponding one-dimensional spectra obtained with the hot-film anemometer. All of the cases show a clear, progressive reduction of both the amplitude and bandwidth of the ambiguity

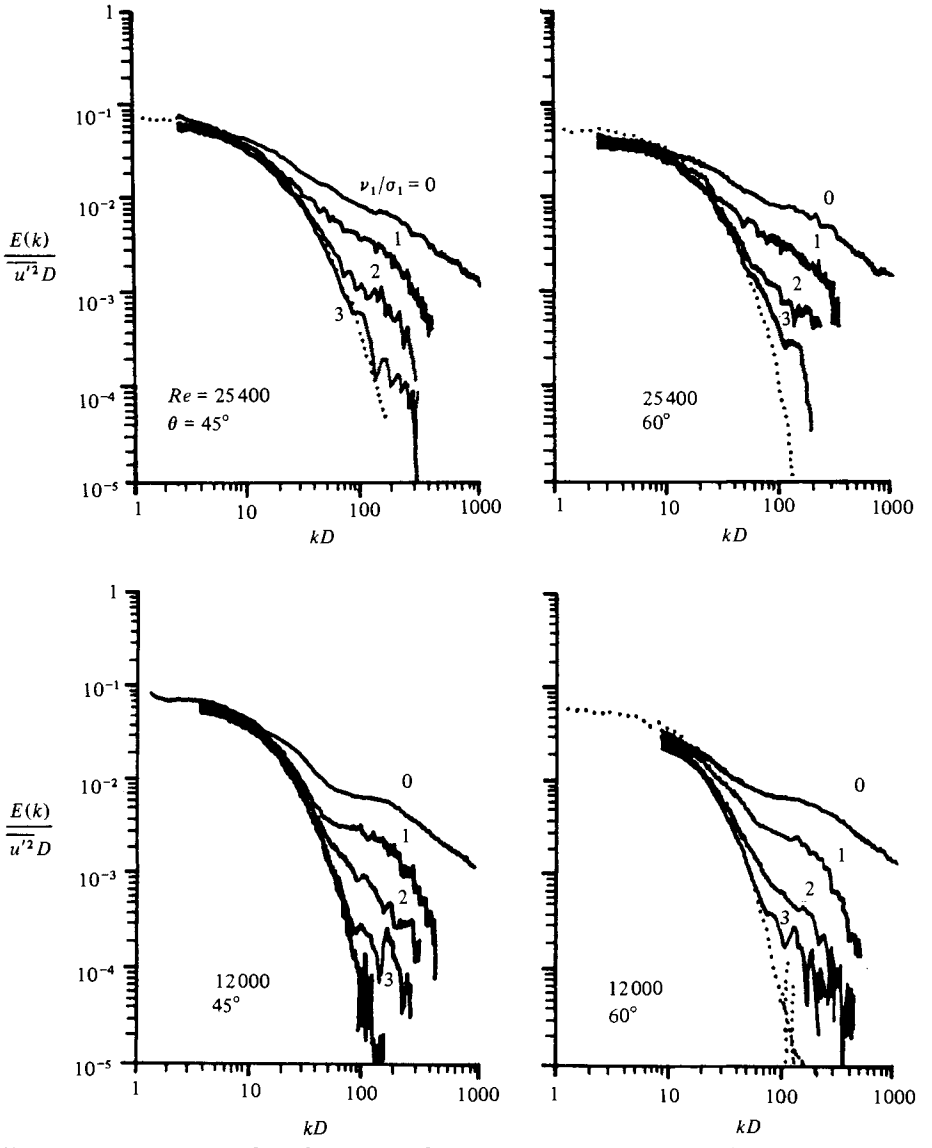

FIGURE 24. Dual-sample-volume turbulence spectra. ——, ultrasonic; · · · · ·, hot-film. Spectral estimates for ultrasonic measurements are based on an average of 200 data records of 2048 points/record with frequency smoothing (Hanning).

spectral components as the spacing between the sample volumes is increased. Simultaneously, the velocity-fluctuation components of the measured spectra, which are nearly identical for each sample volume and are independent of the individual particle populations, are unaffected. Therefore increased amounts of the actual velocity spectra are exposed.

The curves representing large separations typically contain greater variations than those for the more closely spaced sample volumes. Two probable sources of these errors are the statistical variations of the spectral estimate (especially where the non-

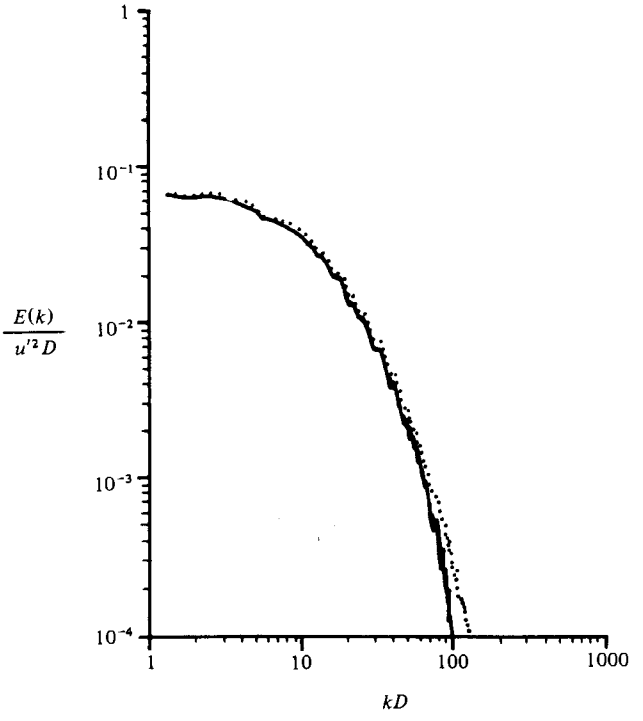

FIGURE 25. Distortion of the spectrum due to sample-volume separation. ——, separated sample volumes; · · · · ·, unseparated sample volumes. Sample volumes separated by $\nu/\sigma_1 = 3, \theta = 45°$, $Re = 25400$.

Gaussian ambiguity components predominate) and low-amplitude noise components in the instrumentation.

As noted in part 1, the separation between the two points of measurement causes the resulting cross-spectrum to deviate from the proper spectrum obtained from a single-point measurement. This error is an important consideration in making dual sample volume measurements. Assuming that the velocity field is isotropic, the amount of distortion in the velocity spectrum can be determined from the Fourier transform of (4.2). For incompressible flow the longitudinal and lateral velocity correlation functions $P_{11}(r, 0, 0)$ and $P_{11}(0, r, 0)$ are related by

$$P_{11}(r, 0, 0) + \tfrac{1}{2} r \frac{\partial}{\partial r}[P_{11}(r, 0, 0)] = P_{11}(0, r, 0). \tag{4.4}$$

For the present situation the $P_{11}(r, 0, 0)$ correlations were computed from the hot-film measurements described in § 3.3. Figure 25 illustrates the distortion of the one-dimensional spectrum for the 'worse case' in the experiments just described. The theoretical spectrum for a single-sample-volume measurement (based on hot film) is shown along with the magnitude of the cross-spectrum of the velocities from the two sample volumes, separated by $\nu/\sigma_1 = 3$. The Reynolds number is 25400 and the Doppler angle is 45°. The distortion takes the form of attenuation of the spectrum at high wavenumbers. However, the error is relatively small in comparison with the statistical variations at the low spectral amplitudes and therefore cannot be observed in the experimental dual-sample-volume measurements (figure 24).

Comparisons of the experimental dual-sample-volume measurements with the cor-

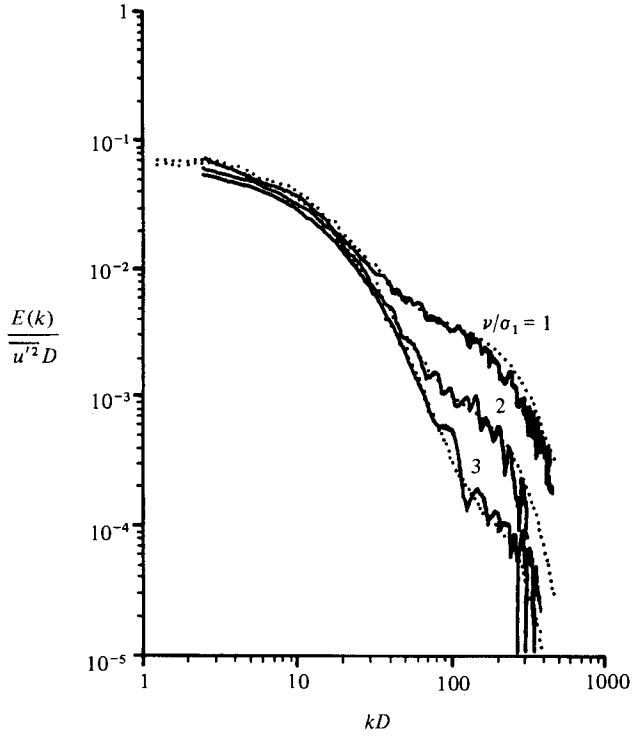

FIGURE 26. Comparison of dual-sample-volume spectral measurements and analytical predictions. ——, ultrasonic; – – –, theoretical; Re = 25400, θ = 45°.

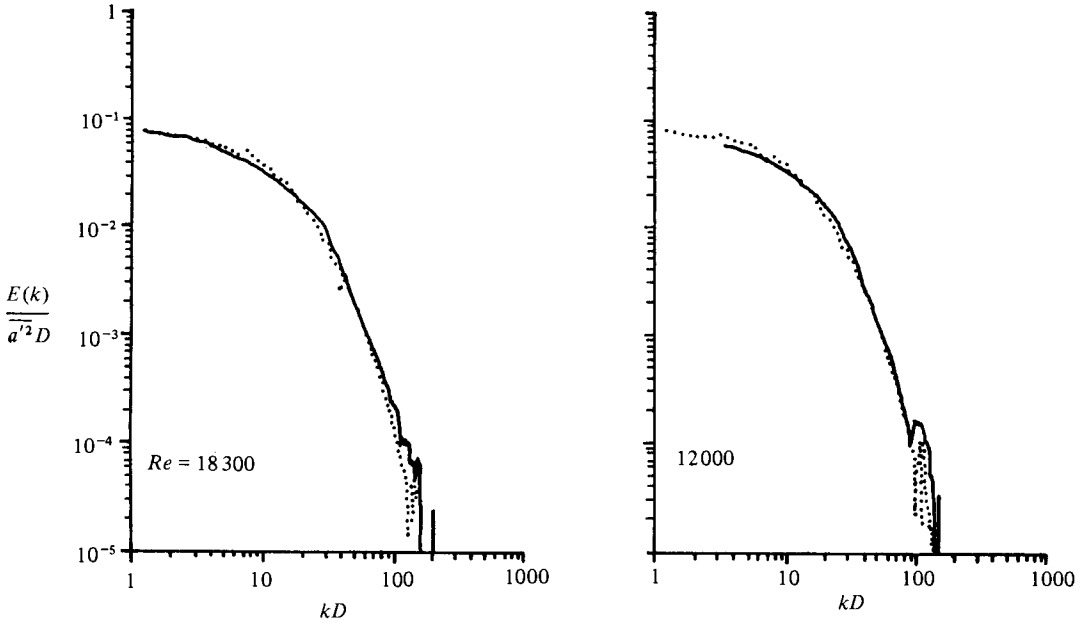

FIGURE 27. Theoretical ambiguity spectrum subtracted from the dual-sample-volume spectral estimates. ——, ultrasonic; · · · · ·, theoretical; θ = 45°, sample volumes separated by ν/σ_1 = 3.

responding modelling equations for turbulent flow ($Re = 25400$, Doppler angle = 45° and sample-volume separations $\nu/\sigma_1 = 1, 2$ and 3) are shown in figure 26. The theoretical curves are based on the hot-film measurements and include the effects of sample-volume spatial averaging (from (3.9) and (3.10)) and the cross-spectrum of the Doppler ambiguity for two separated sample volumes (from (4.3)).

These curves confirm the independence of the ambiguity processes for the two sample volumes from the velocity processes. The agreement between the theory and the experimental data for both the turbulent and laminar measurements demonstrates that (4.3) can be applied to predict the remaining ambiguity for the dual-sample-volume measurements, satisfying the original model assumptions.

In § 3.3 the improved measurement of the one-dimensional velocity spectrum obtained by subtracting the theoretical Doppler ambiguity was described. Although the same restrictions would apply, a similar procedure could be applied to the dual-sample-volume measurements. That is, the theoretical prediction of the remaining ambiguity spectrum could be subtracted from the measured spectrum for which the ambiguity has already been reduced by means of cross-correlation. For a small sample volume the theoretical ambiguity is determined from (4.3), given the values of the mean velocity, the effective sample-volume directivity, the sample-volume separation, and the Doppler angle.

Two examples of this procedure, for $Re = 12000$ and 18300, and $\theta = 45°$, are shown in figure 27. In each case the theoretical ambiguity spectrum has been subtracted from the cross-spectra corresponding to the sample-volume separation of $\nu/\sigma_1 = 3$. Comparing these figures with the measured cross-spectra in which the remaining ambiguity has been retained (figures 25 and 26), the improvement is substantial. Finally, it is interesting to note that the artifacts at the highest wavenumbers appear in both the ultrasonic and the hot-film measurements. This suggests a phenomenon, unrelated to statistical measurement errors, detected by both instruments.

5. Conclusions

An experimental programme, based on the analytical model developed in part 1 of this study, was undertaken to investigate the use of pulsed ultrasound for measurements of turbulent flow. One of the goals of this investigation was to examine the value of the Gaussian-shape approximation for the effective directivity function of a sample volume resulting from a short transmitted pulse in the focal region of a highly focused transducer. The experimental results indicate that this approximation is generally an adequate representation for purposes of predicting sample-volume related effects in the measurement of laminar and turbulent flow. The following major conclusions are based on the results of both the analysis and the experimental program.

(1) It was verified that a decrease in the time of transit of the particles through the sample volume causes a proportional increase in the width of the spectrum of the Doppler signal. This effect was used to measure the characteristic dimensions of the sample volume. The technique was found to be accurate when compared with corresponding echo measurements.

(2) The experimental results confirm the predicted nature of the Doppler ambiguity process in laminar flow. As the velocity increases, the transit time decreases and the Doppler-ambiguity spectrum increases both in magnitude and in bandwidth. The

measured Doppler-ambiguity spectra are in close agreement with the spectral functions predicted in the analysis.

(3) The intensity of turbulence can be evaluated successfully from the width of the Doppler signal spectrum and the description of the effective sample-volume directivity function. Although the measurement error will increase for lower turbulence intensities as the fraction of the spectral broadening caused by turbulence decreases, intensity levels of 3·0–4·5 % were determined accurately.

Much higher levels of turbulence can result in deviations from the 'small-time' assumptions regarding the nature of turbulent motion. This would cause the intensity to be underestimated. Also, the presence of mean velocity gradients and finite off-diagonal terms in the velocity covariance matrix resulting from anisotropic turbulence will result in additional spectral broadening.

(4) The ability of the pulsed ultrasonic velocimeter to measure the one-dimensional turbulence spectrum is greatly limited by the presence of the Doppler-ambiguity process. For the same velocimeter, the level of the ambiguity spectrum relative to that of the velocity spectrum would be even greater for pipes of smaller diameter than those used in this investigation.

The agreement between the theoretical spectra of the detected velocity signal, based on the model and hot-film measurements, and the experimental spectra confirm that the analysis is substantially correct for the cases studied.

The ambiguity effects can be partially removed from the measured spectra by subtracting the theoretical ambiguity spectrum predicted on the basis of transit-time effects. The value of the technique is limited by the necessity of knowing the mean velocity and by inaccuracies both in the theoretical representation of the ambiguity process and in the estimate of the detected velocity signal spectrum. However, a decrease in the level of the ambiguity spectrum of one order of magnitude can realistically be achieved.

(5) A second major effect contributing to decreased accuracy of the velocity spectrum measurement is that of spatial averaging of the velocity field. When the size of the sample volume is large compared with the scale of the turbulence, the amount of attenuation in the measured one-dimensional spectrum is great, particularly at high wavenumbers. Therefore the selection of the size of the sample volume involves a fundamental compromise. As the size is increased the contribution to the ambiguity process of the transit-time effect is diminished but the degree of spatial averaging becomes more severe. In addition, for very large sample volumes, velocity variations induced by turbulence contribute significantly to the Doppler-ambiguity process.

Theoretical predictions of the amount of distortion in the velocity spectra due to finite sample-volume size are in good agreement with the experimental results. These results illustrate, as predicted, that the attenuation of the spectra increases with increasing Reynolds number and wavenumber.

(6) The level and width of the spectrum of the Doppler ambiguity process may be reduced by cross-correlating the signals from two spatially separated sample volumes. The advantage of this technique over that of subtracting the ambiguity process is that it does not rely directly on the accuracy of either a theoretical result or of a spectral estimate. The reduction in the ambiguity spectrum takes place because the ambiguity processes from disjoint particle populations are uncorrelated. An improve-

ment of two to three orders of magnitude in the dynamic range of the spectral measurement can be realistically achieved.

The major governing parameters in this technique are the amount of overlap of the sample volumes and the degree to which the sample volumes are aligned with the direction of the mean flow. For the case of a Gaussian-shaped sample volume, these parameters appear to be adequately taken into account by the results of the theoretical analysis. In using the dual-sample-volume method, care must be taken to avoid large distortion of the cross-spectral magnitude of the spatial average of the velocity field caused by excessive separation of the centres of the sample volumes. The mechanism of this distortion is distinct from that of spatial averaging discussed earlier. For a given sample-volume separation and Doppler angle, the amount of this distortion increases as the scale of turbulence is reduced and/or at higher wavenumbers.

(7) In situations where the cross-spectrum of the remaining ambiguity process can be accurately predicted, a further improvement in the estimation of the one-dimensional spectrum can be made by subtracting this quantity from the cross-spectrum of the detected velocity signals from the two sample volumes. Potentially, this method leads to an improvement of one order of magnitude in addition to that of the cross-spectral method.

REFERENCES

ANGELSEN, B. A. J. & KRISTOFFERSEN, K. 1979 On ultrasonic MTI measurement of velocity profiles in blood flow. *I.E.E.E. Trans. Biomed. Engng* BME **26**, 665–671.

BENDAT, B. S. & PIERSOL, A. G. 1971 *Random Data: Analysis and Measurement Procedures.* Wiley.

BOURKE, P. J., PULLING, D. T., GILL, L. E. & DENTON, W. H. 1968 The measurement of turbulent velocity fluctuations and turbulent temperature fluctuations in the supercritical region by a hot-wire anemometer and a cold wire resistance thermometer. In *Proc. Symp. Heat Transfer and Fluid Dynamics of Near Critical Fluids*, paper 9. Inst. Mech. Engrs, London.

GARBINI, J. L. 1978 Measurement of fluid turbulence based on pulsed ultrasound techniques. Ph.D. dissertation. Dept Mech. Engng, Univ. Washington, Seattle.

GARBINI, J. L., FORSTER, F. K. & JORGENSEN, J. E. 1982 Measurement of fluid turbulence based on pulsed ultrasound techniques. Part 1. Analysis. *J. Fluid Mech.* **118**, 445–470.

GEORGE, W. K. & LUMLEY, J. L. 1973 The laser–Doppler velocimeter and its application to the measurement of turbulence. *J. Fluid Mech.* **60**, 321–363.

GOLDSTEIN, R. J. & KRIED, D. K. 1968 Fluid velocity measurement from the Doppler shift of scattered laser radiation. *Heat Transfer Lab., Dept Mech. Engng, Univ. Minnesota, Minneapolis, Rep.* no. 85.

JENKINS, G. M. & WATTS, D. G. 1968 *Spectral Analysis and its Applications.* Holden-Day.

KOOPMANS, L. H. 1974 *The Spectral Analysis of Time Series.* Academic.

LAUFER, J. 1954 The structure of turbulence in fully-developed pipe flow. *NACA Rep.* no. 1174.

LAWN, C. J. 1971 The determination of the rate of dissipation in turbulent pipe flow. *J. Fluid Mech.* **48**, 477–505.

MONIN, A. S. & YAGLOM, A. M. 1975 *Statistical Fluid Mechanics: Mechanics of Turbulence*, vol. 2. MIT Press.

OPPENHEIM, A. V. & SCHAFER, R. W. 1975 *Digital Signal Processing.* Prentice-Hall.

PENNEL, W. T., SPARROW, W. M. & ECKERT, E. R. G. 1972 Turbulence intensity and time-mean velocity distributions in low Reynolds number turbulent pipe flows. *Int. J. Heat Mass Transfer* **15**, 1067–1074.

PIKE, E. B., JACKSON, P. J. & PAGE, D. I. 1968 Measurement of turbulent velocities from the Doppler shift in scattered laser radiation. *Sci. Instrum.* **1**, 727–730.

RABINER, L. R. & SCHAFER, R. W. 1974*a* Comparison of some IIR and FIR digital filters. *Bell Syst. Tech. J.* **53**, 305–331.

RABINER, L. R. & SCHAFER, R. W. 1974*b* On the behavior of minimax relative error FIR digital differentiators. *Bell Syst. Tech. J.* **53**, 363–390.

RABINER, L. R. & SCHAFER, R. W. 1974*c* On the behavior of minimax FIR digital Hilbert transformers. *Bell Syst. Tech. J.* **53**, 363–390.

RESCH, F. & COANTIC, M. 1969 A study of hot-wire and hot-film anemometers in water. *Houille Blanche* **2**, 151–161.

RICE, S. O. 1949 Statistical properties of a sine wave plus random noise. *Bell Syst. Tech. J.* **27**, 109–157.

SANDBORN, V. A. 1954 Experimental evaluation of momentum terms in turbulent pipe flow. *NACA Tech. Note* no. 3266.